Experimental investigation of the viability of using nano-bubbles for intravascular oxygenation

by
Mynhardt Smit

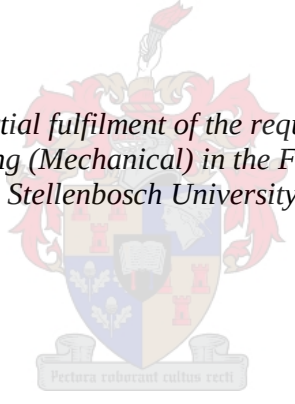

Thesis presented in partial fulfilment of the requirements for the degree of Master of Engineering (Mechanical) in the Faculty of Engineering at Stellenbosch University

Supervisor: Prof Pieter Rousseau Fourie
Co-supervisors: Dr Robert William McClelland Pott
: Mr Cornel De Jongh

March 2020

Declaration

By submitting this thesis elecronically, I declare that the entirety of the work contained therein is my own, original work, that I am the sole author thereof (save to the extent explicitly otherwise stated), that reproduction and publication thereof by Stellenbosch University will not infringe any third party rights and that I have not previously in its entirety or in part submited it for obtaining any qualification.

March 2020

Abstract

In the human body sufficient oxygen supply is of utmost importance. In certain critical conditions the lungs cannot sufficiently supply the human body subsequently other forms of oxygenation are required to potentially save the patients life. Equipment currently available for the purpose of oxygenation is often unaffordable and unavailable. The use of nano-bubbles for intra-vascular oxygenation is envisioned to possibly solve this problem. To determine if this is a viable option to be further investigated, the validation process is broken into multiple phases starting with a basic system that simulates some properties of the pulmonary system, such as flow rate, pipe diameter and systolic pressure while using water as working fluid. This thesis focussed on the first phase and serves as baseline research into the important factors associated with generating nano-bubbles using membranes. The focus of this project is to determine the effects of membrane nominal pore size, oxygen inlet pressure and acoustic interference on oxygenation of a fluid using membranes.

To test the effect of these factors an experimental setup was designed, using water as working fluid, that is used to introduce oxygen bubbles into water through a membrane. Flat sheet and tubular membranes were used to introduce oxygen into the system. Two different inlet manifolds were designed to mount these membranes. Box-Behnken design was used to determine the different combinations of pore size, pressure and frequency that is to be tested and a dissolved oxygen probe was used to measure the levels of dissolved oxygen in the water associated with each combination of variables.

The results obtained during experimentation was analysed, and functions were fitted to the data. The fit of the function was analysed using analysis of variance. The effect of each variable was investigated and discussed. The obtained function was then optimised using a genetic algorithm to determine the expected optimum dissolved oxygen levels.

The results showed evidence that pore size, pressure and frequency influence the level of dissolved oxygen in the mixture. Using the flat sheet membrane, it was determined that the near optimum point is expected to be at 10 nm,

a pressure of 2.8 bar and a frequency of 200 Hz. The effect of bubble size and zeta potential on the level of dissolved oxygen in water was investigated. It was expected that a decrease in bubble diameter would lead to an increase in dissolved oxygen levels. At a zeta potential between -9 mV and -22 mV it was observed that a decrease in bubble diameter does indeed lead to an increase in dissolved oxygen.

Two sets of tests were done using the tubular ceramic membranes. Data from the sets of experiments, using tubular ceramic membranes, were combined, disregarding data obtained using the 100 nm membrane due to leakages affecting the data. It was determined that increasing the pressure, pore size and frequency lead to an increase in DO_2.

As the overarching aim of the project is to be able to sufficiently oxygenate a human intravenously. Considering the evidence obtained, it cannot be concluded that using membranes with nano-scale pores are a viable method for blood oxygenation, as the measured DO_2 obtained in water is relatively low. The main concern, however, is the formation of large oxygen bubbles.

One of the properties of nano-bubbles is that they are neutrally buoyant and that due to their negative surface charge they can stay in a mixture for long periods of time. It is hypothesised that during experimentation, nano-bubbles were generated, but remain stable in the water. As these bubbles possibly did not dissolve the dissolved oxygen levels possibly does not reflect the available oxygen. Further investigation is suggested.

Opsomming

In die menslike liggaam is voldoende suurstofvoorraad uiters belangrik. In sekere kritieke toestande kan die longe nie die menslike liggaam voldoende van suurstof voorsien nie, en dan is ander vorme van oksigenasie nodig om die pasiënt se lewe te red. Toerusting wat tans beskikbaar is met die oog op bloed oksigenasie, is dikwels onbekostigbaar en nie algemeen beskikbaar nie. Die gebruik van nano-borrels vir intravaskulêre oksigenasie word voorgestel om hierdie probleem moontlik op te los.Om te bepaal of dit 'n lewensvatbare opsie is om verder te ondersoek, word die valideringsproses in verskillende fases verdeel, beginnend met 'n basiese stelsel wat 'n paar eienskappe van die pulmonale stelsel simuleer, soos vloeitempo, pypdiameter en sistoliese druk terwyl water gebruik word as werksvloeier. Hierdie tesis fokus op die eerste fase en dien as basislyn-ondersoek na die belangrike faktore wat verband hou met die opwekking van nano-borrels met behulp van membrane. Die fokus van hierdie projek is om die effekte van membraan nominale poriegrootte, suurstofinlaatdruk en akoestiese interferensie op oksigenering van vloeistof met behulp van membrane te bepaal.

Om die effek van hierdie faktore te toets, was 'n eksperimentele stelses ontwerp, waar water as werkvloeistof gebruik was, om suurstofborrels deur die membraan in die water in te bring. Platvel- en buisvormige membrane was gebruik om suurstof in die stelsel in te voer. Twee verskillende inlaatspruitstukke was ontwerp om hierdie membrane te monteer. Box-Behnken-ontwerp was gebruik om die verskillende kombinasies van poriegrootte, druk en frekwensie wat getoets moet word te bepaal, en 'n opgeloste suurstof meter word gebruik om die vlakke van opgeloste suurstof in die water, wat met elke kombinasie van veranderlikes geassosieer word, te meet.

Die resultate wat tydens eksperimentering verkry was, was ontleed, en 'n funksie was op die data gepas. Die pas van die funksie was geanaliseer met behulp van variansie-analise. Die effek van elke veranderlike was ondersoek en bespreek. Die verkrygde funksie was toe geoptimaliseer met behulp van 'n genetiese algoritme om die verwagte optimale opgeloste suurstofvlakke te bepaal.

Die resultate het bewys dat poriegrootte, druk en frekwensie die vlak van opgeloste suurstof in die mengsel benvloed. Deur die gebruik van die platvelmembrane is daar bepaal dat die naaste optimale punt na verwagting by n poriegrootte van 10 nm sal wees, 'n druk van $2,8$ bar en 'n frekwensie van 200 Hz. Die effek van borrelgrootte en zeta-potensiaal op die vlak van opgeloste suurstof in water is ondersoek. Daar word verwag dat 'n afname in borreldiameter sou lei tot 'n toename in opgeloste suurstofvlakke. By 'n zeta-potensiaal tussen -9 mV en -22 mV is daar waargeneem dat 'n afname in borreldiameter lei wel tot 'n toename in opgeloste suurstof.

Twee stelle toetse was met behulp van die buisvormige keramiek membrane gedoen. Data van die stelle eksperimente, met behulp van buisvormige keramiek membrane, was gekombineer, met uitsluiting van data wat verkry was met behulp van die 100 nm membraan weens lekkasies wat die data benvloed. Daar was bepaal dat die verhoging van die druk, poriegrootte en frekwensie lei tot 'n toename in DO_2. Vir hierdie gekombineerde stel data was vasgestel dat die suurstofdruk en die frekwensie van die klankgolf wat die stelsel vibreer die mees beduidende invloed het op die vlak van DO_2.

Die oorkoepelende doel van die projek is om 'n vir mens genoegsame suurstof binneaars te kan toedien. Met inagneming van die bewyse wat verkry was, kan daar nie afgelei word dat die gebruik van membrane met nanoskaalsporiee 'n lewensvatbare metode is om suurstof in bloed te bewerkstellig nie, aangesien die vlak van DO_2 wat in water verkry is, relatief laag is. Die grootste bekommernis is egter die vorming van groot suurstofborrels op sekere plekke op die membraan.

Een van die eienskappe van nano-borrels is dat hulle neutraal dryf en dat hulle as gevolg van hul negatiewe oppervlaktelading gedurende 'n lang periode in 'n mengsel kan bly, soos gellustreer deur die eksperiment wat deur Meegoda *et al.* (2018) gedoen is. Daar word veronderstel dat nano-borrels tydens eksperimentering gegenereer word en stabiel in die water bly. Aangesien dit moontlik is dat hierdie borrels nie oplos nie, weerspiel die opgeloste suurstofvlakke moontlik nie die totale beskikbare suurstof nie. Verdere navorsing word voorgestel.

Contents

Contents vi

List of Figures ix

List of Tables xiv

1 Introduction 1
- 1.1 Objectives . . . 2
- 1.2 Motivation . . . 3

2 Literature Review 4
- 2.1 The pulmonary system . . . 4
- 2.2 Known oxygenation methods . . . 7
  - 2.2.1 Extracorporeal Membrane Oxygenation . . . 7
  - 2.2.2 Intravascular Oxygenator . . . 8
- 2.3 Mass transfer . . . 9
  - 2.3.1 Steady-State molecular diffusion . . . 9
  - 2.3.2 Mass transfer across a fluid-fluid interface . . . 10
- 2.4 Use of flat sheet membranes for oxygenation of water . . . 11
- 2.5 Nano-bubbles . . . 12
- 2.6 Generation of nano-bubbles by means of ceramic membranes . 14
- 2.7 Conclusion: Literature review . . . 19

3 Design of Experiments 21
- 3.1 Response surface methodology . . . 22
- 3.2 Experimental Setup . . . 23
- 3.3 Inlet manifold using flat sheet membranes . . . 24
  - 3.3.1 Working principle of the inlet manifold using a flat sheet membrane . . . 25
  - 3.3.2 Inlet manifold design for a setup using a flat sheet membrane . . . 26
  - 3.3.3 Design of the pressure vessel for the inlet manifold . . . 27
- 3.4 Inlet manifold using tubular ceramic membranes . . . 28

3.4.1 Working principle of the inlet manifold using a tubular ceramic membrane . . . 28
3.4.2 Inlet manifold design for a setup using a tubular ceramic membrane . . . 29
3.4.3 Pressure vessel for the second generation design . . . 30
3.5 Experimental method . . . 31
3.5.1 Oxygen probe calibration and measurements . . . 31
3.5.2 Important zero-readings . . . 31
3.5.3 Experimental procedure . . . 31
3.5.4 Particle size and zeta potential determination . . . 32
3.6 Conclusion: Design of experiment . . . 32

4 Membrane specifications **33**
4.1 Flat sheet membranes . . . 33
4.1.1 Flat sheet membrane specifications . . . 33
4.1.2 Verification of membrane pore size . . . 35
4.2 Tubular ceramic membranes . . . 37
4.2.1 Tubular ceramic membrane specifications . . . 37
4.3 Conclusion: Membrane specifications . . . 38

5 Results **39**
5.1 Generating bubbles using flat sheet membranes . . . 39
5.1.1 Box-Behnken design for experimental variable selection 40
5.1.2 Experimental measurements and observations . . . 42
5.1.3 Response surface methodology . . . 43
5.1.4 Optimisation of response surface . . . 53
5.1.5 Conclusion: Generating bubbles using flat sheet membranes . . . 56
5.2 Generating bubbles using tubular ceramic membranes . . . 57
5.2.1 Box-Behnken design for experimental variable selection 57
5.2.2 Experimental measurements and observations . . . 59
5.2.3 Experimental measurements and observations . . . 59
5.2.4 Response surface methodology . . . 60
5.2.5 Optimisation of response surface using a genetic algorithm 66
5.2.6 Conclusion: Generating bubbles using tubular ceramic membranes . . . 73
5.3 Conclusion: Results . . . 74

6 Conclusion **75**

7 Recommendations **77**
7.1 PhD proposal . . . 77

Bibliography **80**

A Statistical analysis results tables **a**
A.1 Summary and ANOVA results for experimental setup using flat sheet membranes . . . . . a
A.2 Summary and ANOVA results for experimental setup using tubular ceramic membranes c

B Pressure vessel design **d**

C Scanning electron microscope results **f**

List of Figures

1.1 Breakdown of the phases required to develop a intra-vascular oxygenation device. The focus of this project is Phase 1. 2

2.1 Diagram indicating oxygen transport from atmosphere to mitochondria. Partial pressures are indicated between brackets in kPa 5
2.2 Plot of cardiac index (CI) over age. The data represents measurements of healthy males and females of different ages. The mean of CI for males is given by the function, $y = -0.0095 \cdot age + 3.275$ and for females, $y = -0.0072 \cdot age + 3.423$ 7
2.3 Diagram indicating the circuitry of Extracorporeal Membrane Oxygenation 8
2.4 Film theory for mass transfer from a fluid-fluid interface into a liquid 10
2.5 Schematic diagram of the experimental setup used by Maynard (2017) to observe bubble formation and behaviour when using different membranes to introduce oxygen into water 11
2.6 Photograph taken showing the experimental setup used by Maynard (2017) to observe bubble formation and behaviour when using different membranes to introduce oxygen into water 11
2.7 Plot of zeta potential of nano-bubbles over time for fluids with different pH values 13
2.8 Plot of bubble size of nano-bubbles over time for fluids with different pH values 13
2.9 A schematic diagram and photo of the experimental setup used by Ahmed *et al.* (2018) to generate nano-bubbles 14
2.10 Plots of hydrodynamic diameter over time of air nano-bubbles at different inlet pressures 16
2.11 Plots of zeta potential over time of air nano-bubbles at different inlet pressures 17
2.12 Plot indicating the change in the dissolved oxygen level as oxygen is injected into the water over time 18

2.13 Particle size distribution measured of air nano-bubbles that were generated using two different membranes with a 100 *nm* and 1000 *nm* nominal pore size 18
2.14 Zeta potential (ZP) measurements of air nano-bubbles that were generated using two different membranes, one with a 100 *nm* and a 1000 *nm* nominal pore size 18

3.1 The individual steps involved in response surface methodology, which is the method used to design the experiments 22
3.2 Schematic diagram of experimental setup showing water flow control (A), buffer tank (B), oxygen and water interface (C), oxygen inlet and flow control (D) and dissolved oxygen probe (E) 23
3.3 A 3D Rendering of the buffer tank assembly, as drawn using Autodesk Inventor, with the inlet connected to a float valve which ensures a constant water level in the tank. 24
3.4 Sectional view of the inlet manifold assembly with the flat sheet membrane mounted between the two flanges. 25
3.5 A rendering of the inlet manifold assembly. The assembly consists of a 3D printed inlet tube and a stainless steel flange fitted together using pipe clamps 26
3.6 Exploded views of the inlet manifold assembly,at different angles, showing the oxygen inlet pressure vessel, the silicon gaskets, the 3D printed inlet tube and the required fasteners 27
3.7 Sectional view of the inlet manifold, using a ceramic membrane, indicating water and oxygen flow in the experimental setup . . . 28
3.8 Exploded view of the revised design of the inlet manifold assembly consisting of the pressure vessel, membrane housing and membrane 29
3.9 Exploded view of the adjustable section of the inlet manifold. . 30
3.10 Pressure vessel mounted to the inlet assembly 30

4.1 Plot of Molecular Weight Cut-off vs Nominal Pore Size in nanometer generated using MATLAB (2019) 34
4.2 Scanning electron microscope image of TRISEP® UB70 35
4.3 Scanning electron microscope image of SelRO® MPS-34 35
4.4 Scanning electron microscope image of NADIR® UH050 P . . . 35
4.5 Scanning electron microscope image of NADIR® UH010 P . . . 35
4.6 Illustration of a gas bubble forming through a crack 37

5.1 The TRISEP® UB70 membrane fractured at a pressure of just over 4 *bar* 41
5.2 3D Plot representing the variable value combinations for the set of experiments, as determined using Box-Behnken design 41

5.3 Surface plot of dissolved oxygen over pressure and pore size, with blue markers indicating measured data 44
5.4 Surface plot of dissolved oxygen over frequency and pore size, with blue markers indicating measured data 44
5.5 Surface plot of dissolved oxygen over frequency and pressure, with blue markers indicating measured data 45
5.6 Surface plot of dissolved oxygen over pressure and pore size at 200 Hz 46
5.7 Surface plot of dissolved oxygen over pressure and pore size at 2 600 Hz 46
5.8 Surface plot of dissolved oxygen over pressure and pore size at 5 000 Hz 47
5.9 Surface plot of dissolved oxygen over frequency and pore size at 1 bar 48
5.10 Surface plot of dissolved oxygen over frequency and pore size at 2.25 bar 48
5.11 Surface plot of dissolved oxygen over frequency and pore size at 3.5 bar 48
5.12 Surface plot of dissolved oxygen over frequency and pressure at 10 nm 49
5.13 Surface plot of dissolved oxygen over frequency and pressure at 12.5 nm 49
5.14 Surface plot of dissolved oxygen over frequency and pressure at 15 nm 49
5.15 Pareto chart of standardized effects 50
5.16 Surface plot of dissolved oxygen over bubble size and zeta potential 53
5.17 Surface plot of dissolved oxygen over bubble size and zeta potential with blue markers indicating measured data 53
5.18 Surface plot of dissolved oxygen over bubble size and zeta potential 53
5.19 Plot of the best individual and the mean of each generation . . . 55
5.20 Plot of the best, worst and mean scores for each generation . . . 55
5.21 3D Plot representing the variable value combinations for the set of experiments, as determined using Box-Behnken design 58
5.22 Surface plot of dissolved oxygen over pressure and pore size, with blue markers indicating measured data 61
5.23 Surface plot of dissolved oxygen over frequency and pore size, with blue markers indicating measured data 61
5.24 Surface plot of dissolved oxygen over frequency and pressure, with blue markers indicating measured data 61
5.25 Surface plot of dissolved oxygen over pressure and pore size at 200 Hz 62
5.26 Surface plot of dissolved oxygen over pressure and pore size at 2 600 Hz 62

5.27 Surface plot of dissolved oxygen over pressure and pore size at 5 000 Hz . . . 62
5.28 Surface plot of dissolved oxygen over frequency and pore size at 1 bar . . . 63
5.29 Surface plot of dissolved oxygen over frequency and pore size at 2.5 bar . . . 63
5.30 Surface plot of dissolved oxygen over frequency and pore size at 4 bar . . . 63
5.31 Surface plot of dissolved oxygen over frequency and pressure at 50 nm . . . 64
5.32 Surface plot of dissolved oxygen over frequency and pressure at 100 nm . . . 64
5.33 Surface plot of dissolved oxygen over frequency and pressure at 200 nm . . . 65
5.34 Pareto chart of standardized effects . . . 65
5.35 Plot of the best individual and the mean of each generation . . . 67
5.36 Plot of the best, worst and mean scores for each generation . . . 67
5.37 Surface plot of dissolved oxygen over pressure and pore size, with blue markers indicating measured data . . . 70
5.38 Surface plot of dissolved oxygen over frequency and pore size, with blue markers indicating measured data . . . 70
5.39 Surface plot of dissolved oxygen over frequency and pressure, with blue markers indicating measured data . . . 70
5.40 Pareto chart of standardized effects . . . 71
5.41 Surface plot of dissolved oxygen over frequency and pressure, obtained from combining the two sets of data recorded using tubular ceramic membranes . . . 71
5.42 Surface plot of dissolved oxygen over pressure and pore size, obtained from combining the two sets of data recorded using tubular ceramic membranes . . . 71
5.43 Side view of a surface plot of dissolved oxygen over frequency and pore size, obtained from combining the two sets of data recorded using tubular ceramic membranes . . . 72

7.1 Schematic diagram of the proposed experimental setup including buffer tank (A), heat exchanger (B), positive displacement pump (C), oxygen inlet manifold (D), dissolved oxygen probe (E), oxygen tank with regulator (F) and nitrogen sparger setup (G) . . . 78

B.1 SANS 347-2012 Graph for vessels, Non-dangerous gas . . . d
B.2 Finite element analysis of the pressure vessel indicating the maximum and minimum safety factor at a pressure of 10 *bar* . . . e

C.1 Scanning electron microscope image of TRISEP® UB70 . . . . . f
C.2 Scanning electron microscope image of SelRO® MPS-34 . . . . . g
C.3 Scanning electron microscope image of NADIR® UH050 P . . . h
C.4 Scanning electron microscope image of NADIR® UH010 P . . . h

List of Tables

2.1 Specifications of the various membranes investigated by Maynard (2017) during experimentation 12
2.2 Results optained using PIV during experimental testing Maynard (2017) 12
2.3 Dimensions and nominal pore sizes of the respective membranes used in the experimental setup 15

4.1 Specifications of sourced membranes as given by suppliers, showing membrane chemistry and Molecular Weight Cut-off or nominal pore size 34
4.2 Comparison of expected and actual pore size 36
4.3 Specifications of the tubular ceramic membranes 37

5.1 The ranges of the variables as used in Box-Behnken 40
5.2 Experimental data at a water flowrate of 5 L/min 43
5.3 Comparison of results obtained using a Genetic Algorithm with different population sizes and number of generations 54
5.4 The ranges of the variables as used in Box-Behnken 57
5.5 Experimental data at a water flowrate of 3 L/min 59
5.6 Comparison of results obtained using a Genetic Algorithm with different population sizes and number of generations 66
5.7 The ranges of the variables as used in Box-Behnken 68
5.8 Experimental data at a water flowrate of 3 L/min 68

A.1 Results table of the function fit to the data obtained using a flat sheet membrane . . . . . a
A.2 ANOVA table of the function fit to the data obtained using a flat sheet membrane . . . . . b
A.3 ANOVA of the function as described by Equation 5.3 . . . . . b
A.4 Results table of the function as described by Equation 5.7 . . . c
A.5 ANOVA of the function as described by Equation 5.7 c

Chapter 1

Introduction

In the human body sufficient oxygen supply is of the utmost importance. In certain critical conditions the lungs cannot sufficiently supply oxygen in the human body and then other forms of oxygenation are required to potentially save the patient's life. Equipment currently available for the purpose of oxygenation, such as extracorporeal membrane oxygenation (ECMO), is often very expensive, inaccessible or insufficient in supplying the required amount of oxygen. Therefore, the development of an intravascular oxygenation membrane is suggested.

The idea of using nano-scale oxygen bubbles for intravascular oxygenation is envisioned as a possibility, due to numerous claimed properties of nano-bubbles that could be advantageous for blood oxygenation, such as the small diameter, a negative surface charge called zeta-potential that reduces coagulation of bubbles and neutral buoyancy (NanoMAX, 2019). The smaller diameter could be advantageous as these bubbles will have a larger total contact surface area compared to larger bubbles with the same total volume. Large bubbles forming in blood could lead to serious illness or even death, therefore the negative surface charge, inhibiting coalescence of bubbles, could be of great advantage for blood oxygenation.

To determine if nano-bubbles are a viable method to use for blood oxygenation, a number of phases, Figure 1.1, are set out. The focus of this project is Phase 1. Phase 1 serves as baseline research into the important factors associated with generating nano-bubbles using membranes. The focus of this phase is to determine the effects of membrane nominal pore size, oxygen inlet pressure and acoustic interference on oxygenation of a fluid using membranes. As this is a baseline investigation, water is used as a working fluid instead of blood.

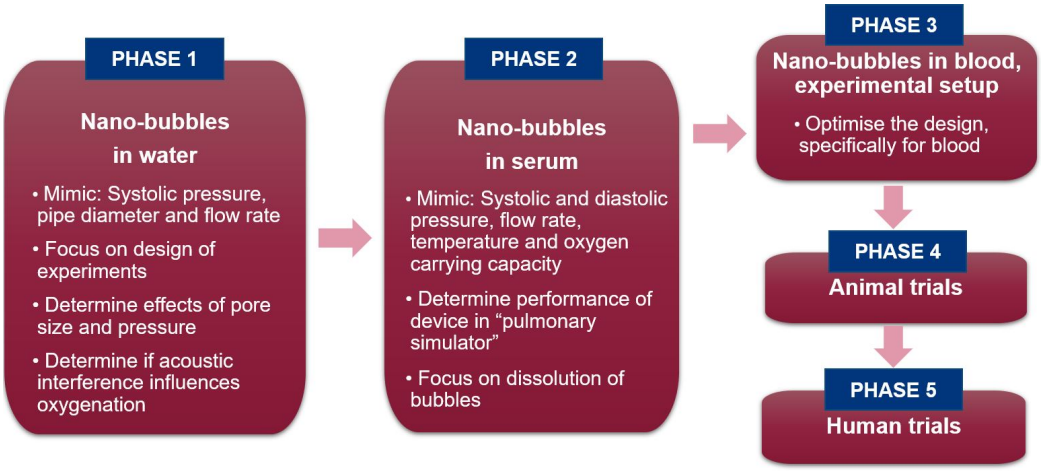

Figure 1.1: Breakdown of the phases required to develop a intra-vascular oxygenation device. The focus of this project is Phase 1.

This thesis consists of 6 chapters. In Chapter 2 an in-depth literature review is given of oxygen transport in the pulmonary system, current state of the art regarding blood oxygenation, the properties of nano-bubbles and previous work done within the field. Chapter 3 gives a description of the design of experiments. The experimental setup is described, and the purpose of each component thereof is discussed. The designs of two inlet manifolds are discussed, one using a set of flat sheet membranes and the other a tubular ceramic membrane.

In Chapter 4 the two different types of membranes used to oxygenate water are discussed. The properties of each are discussed and validated. Chapter 5 focusses on the selection of the values of the sets of variables used for the experiments. The results and observations are discussed and analysed. Functions are fit to the data of the different experiments conducted and these functions are analysed using analysis of variance (ANOVA), to determine how well the function describes the data. These functions are then optimised, using a genetic algorithm, to determine the expected near optimum. The thesis is concluded in Chapter 6, where the thesis is discussed as a whole and suggestions are made for future work and research.

1.1 Objectives

The overarching aim of this project is to sufficiently oxygenate a human body intravenously in a manner that is safe, cost effective and accessible. To achieve

this is not in the scope of this project. To get one step closer to achieving this it is firstly important to determine the effect that membrane pore size, oxygen inlet pressure and sonic interference have on oxygenation of water using nano-bubbles.

The main objectives of this project are:

1. To do a *literature study* that investigates the pulmonary system, current state of the art, the properties of nano-bubbles and previous work done regarding membrane oxygenation.

2. To design an *experimental setup*, with water as a working fluid, that mimics the critical properties of the pulmonary system.

3. To design an *inlet manifold* to introduce oxygen bubble into the water through a membrane.

4. To determine if the nominal pore size of the membrane and the oxygen inlet pressure have an effect on the oxygenation of the water and what that effect is.

5. To determine if sonic interference has an effect on the oxygenation of the working fluid.

1.2 Motivation

In the field of Biomedical Engineering the main motivation should be to use acquired engineering knowledge and skills to the advantage of humanity, by improving health and quality of life. The development of an intravenous oxygenation device, that is more cost efficient, accessible and more mobile than current devices, would lead to more people being helped and possibly lives being saved.

Determining the effect of various factors, such as the membrane nominal pore size, oxygen inlet pressure and sonic interference, on the oxygenation of water, would give insight into oxygenation using nano-bubbles as a whole. It will also give insight into the formation of nano-bubbles. This insight into oxygenation and bubble formation could be used to determine if the possibility of oxygenating a human body, intravenously, using nano-bubbles should be investigated further.

Chapter 2

Literature Review

The literature review gives information on the pulmonary system, it's function and what the system output is. Previous work done is discussed and implements that are already available are considered. The aim of the literature review is to give an oversight of the background information that should be investigated in more detail once the project commences.

2.1 The pulmonary system

An overview of the pulmonary system function is presented and the processes associated with oxygen transport and transfer are investigated. The purpose of investigating the pulmonary system is to determine, in effect, the engineering specifications thereof in order to translate it to an experimental setup. For instance, it is important to know the oxygen requirements of the human body to determine if it is likely, when considering the results of the experiment using water, that sufficient oxygen levels could be reached when using blood.

The cells in the human body greatly depend on oxygen for aerobic metabolism and cell integrity. Cells and tissue cannot store oxygen, therefore a constant supply of oxygen is required. The pulmonary system exists to ensure continuous oxygen supply. Should the supply of oxygen be interrupted or reduced it could lead to cell damage, organ failure and death (Treacher *&* Leach, 1998).

Oxygen transport is the process by which oxygen from the atmosphere is supplied to the tissues. Figure 2.1 below is a representation of oxygen transport for a healthy person weighing 75 kg.

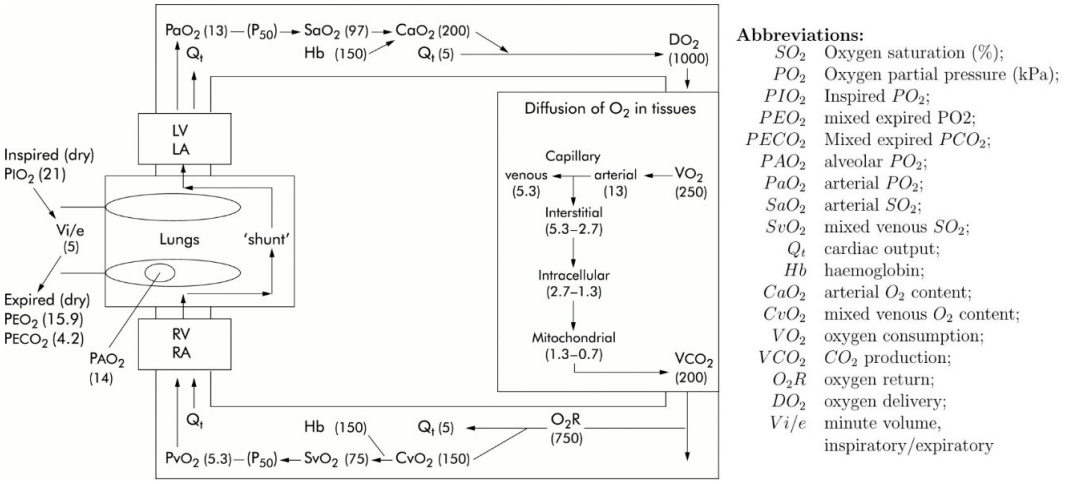

Figure 2.1: Diagram indicating oxygen transport from atmosphere to mitochondria. Partial pressures are indicated between brackets in kPa (Leach, 2002)

As the overarching goal is to sufficiently oxygenate the human body it is important to know what the oxygen consumption of the human body is. The total amount of oxygen consumed by the human body per minute is calculated as follows, where V_{O_2} is oxygen consumption, Q_t is volume flow rate and $(C_{aO_2} - C_{VO_2})$ the difference between arterial and mixed venous oxygen content:

$$V_{O_2} = Q_t \cdot (C_{aO_2} - C_{VO_2}) \tag{2.1}$$

As seen in Equation 2.1 the global oxygen consumption is the difference between the arterial and venous oxygen content, multiplied by the cardiac output. For the case of a 75 kg person, as indicated in figure1, the global oxygen consumption can be calculated as follows:

$$V_{O_2} = 5\frac{l}{min}\left(200\frac{ml}{l} - 150\frac{ml}{l}\right)$$

$$= 250\frac{ml}{min} \tag{2.2}$$

The value for oxygen consumption, as calculated in Equation 2.2, is important as this is the ideal goal for oxygenators.

An important consideration is the oxygen carrying capacity of blood which determines the amount of oxygen delivered. The equation used to determine

the rate of oxygen delivery is,

$$DO_2 = CO \cdot (1.39 \cdot Hb \cdot SaO_2 + (0.003 \cdot PaO_2)) \tag{2.3}$$

Where CO is the cardiac output in liters per minute, Hb is the Haemoglobin concentration in grams per liter, SaO_2 is the Haemoglobin oxygen saturation expressed as a fraction and PaO_2 the arterial oxygen tension. The oxygen binding capacity of Haemoglobin is 1.39 mL/g. The solubility coefficient in plasma is 0.003. This means for every 1 $mmHg$ of oxygen tension, 0.003 mL of oxygen gas is dissolved in 100 mL of blood (Fourie, 2017).

The volume flow rate of the pulmonary system is an important parameter to take into consideration when designing a experimental setup. The volume flow rate should be mimicked as this could influence the performance of an intravenous device significantly.

In research done by Carlsson *et al.* (2012), Cardiovascular Magnetic Resonance was used to determine the cardiac index (CI) of a group of people consisting of males and females. The recorded data is plotted in Figure 2.2 and functions are fitted that represent CI in males and females. It was determined that the average CI for women was 3.1 $L/min/m^2$ and 3.2 $L/min/m^2$ for men. The cardiac index of a person can be expressed as cardiac output (CO) divided by body surface area.

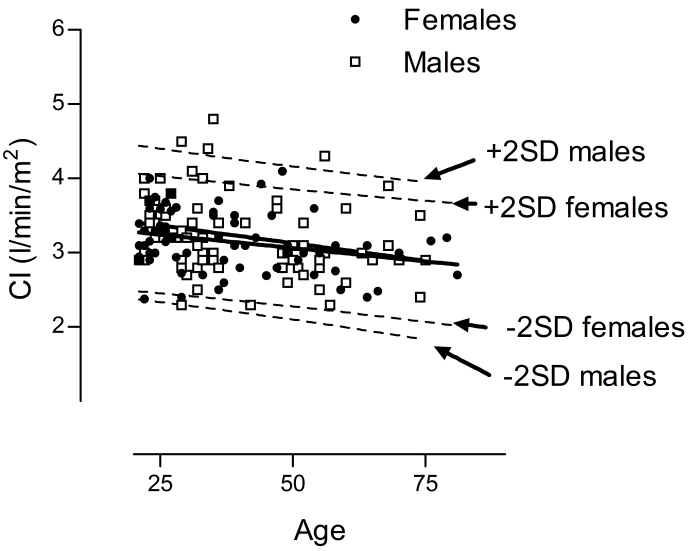

Figure 2.2: Plot of cardiac index (CI) over age. The data represents measurements of healthy males and females of different ages. The mean of CI for males is given the function, $y = -0.0095 \cdot age + 3.275$ and for females, $y = -0.0072 \cdot age + 3.423$ (Carlsson *et al.*, 2012)

2.2 Known oxygenation methods

When developing a device, it is important to consider devices that are available and to consider the strengths and weaknesses of these devices. This section considers devices that were developed and tested. It includes extracorporeal membrane oxygenation (ECMO) that is used in industry as well as the intravascular oxygenation (IVOX) device.

2.2.1 Extracorporeal Membrane Oxygenation

Extracorporeal Membrane Oxygenation (ECMO) has been used since 1970 to support patients who suffer pulmonary or cardiac distress (Sweeney, 2019). ECMO makes use of cannulas (special tubes) that are inserted into the patients blood vessels that go directly into the heart or bloodstream. Blood is transferred out of the body using a peristaltic pump, pumped through an oxygenation membrane where the blood is oxygenated, heated back to body temperature by means of a heat exchanger and returned to the patients body (Texas, 2018). This is illustrated in Figure 2.3 (Sweeney, 2019).

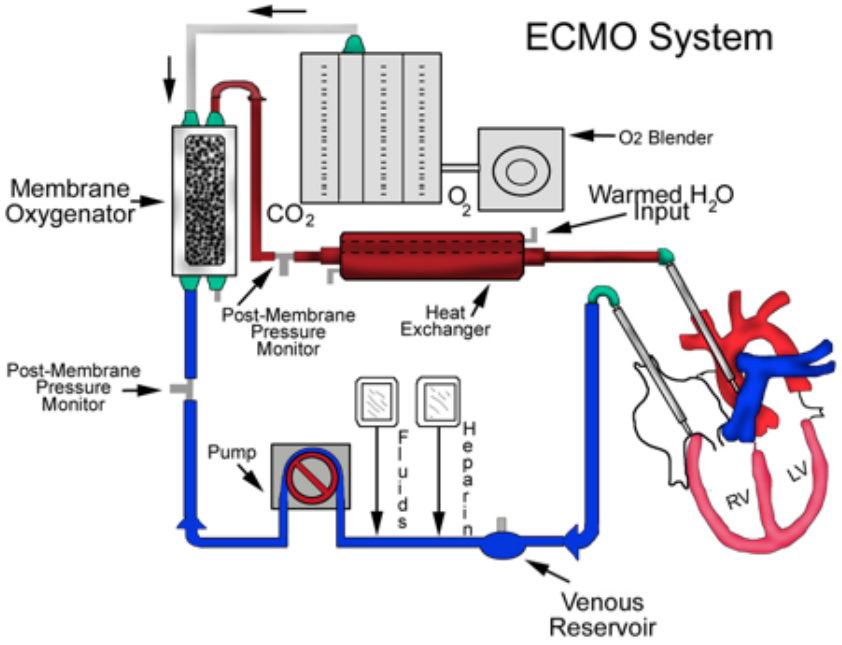

Figure 2.3: Diagram indicating the circuitry of Extracorporeal Membrane Oxygenation (Sweeney, 2019)

Two types ECMO are available, VV(veno-venous) and VA(veno-arterial). VV is used as a lung bypass to treat severe respiratory distress. Oxygen is drained from the body from the right atrium, oxygenated and then returned to the body through the right side of the heart, at the right atrium. VA is used to bypass the entire cardio-pulmonary system, giving the heart and lungs time to recover. Blood is drained from the right atrium, oxygenated using a membrane oxygenator and pumped back into the proximal aorta via the return cannula (Stoecklein *et al.*, 2019).

2.2.2 Intravascular Oxygenator

Intravascular Oxygenator (IVOX) is a membrane oxygenator consisting of a bundle of hollow fibres. It serves as respiratory support for patients with acute respiratory failure. The device is surgically inserted into the inferior or superior vena cava. Gas exchange occurs through the hollow fibres. This is driven using a vacuum pump. Clinical test that were done concluded that IVOX is safe but does not deliver sufficient amounts of oxygen as it only delivers 25% of the basic requirement of a human body. Limitations of IVOX include a moderate rate of gas exchange, difficulty in implanting the device and device malfunction. A number of health risks associated with the use IVOX include thrombotic

complications, the device obstructing blood flow and gas leakages into the blood (Yuan, 2016).

2.3 Mass transfer

Mass transfer from a gas to a liquid is investigated to gain understanding of the mechanisms associated with oxygen dissolution in water.

2.3.1 Steady-State molecular diffusion

Henley *et al.* (2011) gives the example of dyed water in a tubular glass container. Clear water is added to the dyed water and a sharp boundary between the two is observed. As time passes the colour of the volume closest to the original clear-dyed water interface becomes less coloured than the bottom dyed region. The motion of each dye molecule is random, colliding with water molecule but also with other dye molecules. This continues until the mixture is uniformly coloured. Based on these observations it was concluded that mass transfer by means of molecular diffusion occurs because of a concentration gradient. This diffusion occurs in the direction of decreasing concentration and is proportional to the area normal to diffusion direction. The net transfer stops when concentrations are uniform within the mixture (Henley *et al.*, 2011).

Based on these observations Fick postulated that diffusion can be compared to Fourier's first law of heat conduction,

$$q_z = -k\frac{dT}{dz} \tag{2.4}$$

where q_z is the conduction heat flux, k is the thermal conductivity and dT/dz is the temperature gradient (Henley *et al.*, 2011). Fick's analogy to this, for diffusion of a mixture of A and B, is described by,

$$J_{A_z} = -D_{AB}\frac{dc_A}{dz} \tag{2.5}$$

$$J_{B_z} = -D_{BA}\frac{dc_B}{dz} \tag{2.6}$$

where J_{A_z} and J_{A_z} represents the molar flux of A and B, respectively, due to diffusion. The mutual diffusion coefficient is represented by $-D_{AB}$ and $-D_{BA}$ and the concentration gradient for A and B is represented by dc_A/dz and dc_B/dz (Henley *et al.*, 2011).

2.3.2 Mass transfer across a fluid-fluid interface

Film theory describes mass transfer from a gas to a liquid. The theory suggests that the gas, with concentration c_{A_i}, must diffuse through a layer of thickness δ_L to the film-bulk liquid interface, with a bulk-average concentration c_{A_b}. Line c_{A_i} - c_{A_b}, as seen in Figure 2.4, represents the linear decline in concentration (Henley *et al.*, 2011).

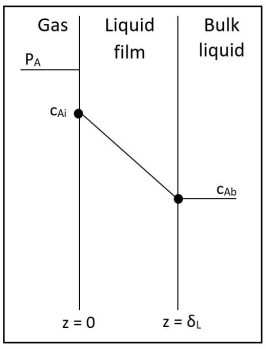

Figure 2.4: Film theory for mass transfer from a fluid-fluid interface into a liquid (Henley *et al.*, 2011)

The film acts as a resistance to diffusion as it is assumed that all the gas diffuses through this film. Integration of Fick's first law, as seen in Equation 2.5, gives

$$\begin{aligned} J_A &= \frac{D_{AB}}{\delta}(c_{A_i} - c_{A_b}) \\ &= \frac{cD_{AB}}{\delta}(x_{A_i} - x_{A_b}) \end{aligned} \tag{2.7}$$

If the liquid is dilute, the bulk-flow effect can be neglected, leading to a linear concentration gradient, as seen in Figure 2.4. The molar flux, N_A, is given by

$$\begin{aligned} N_A &= \frac{D_{AB}}{\delta}(c_{A_i} - c_{A_b}) \\ &= \frac{cD_{AB}}{\delta}(x_{A_i} - x_{A_b}) \end{aligned} \tag{2.8}$$

If the bulk-flow effect cannot be neglected, the molar flux is given by

$$N_A = \frac{cD_{AB}}{\delta} ln \left[\frac{1 - x_{A_i}}{1 - x_{A_i}} \right]$$
$$= \frac{cD_{AB}}{\delta(1 - x_A)_{LM}} (x_{A_i} - x_{A_b}) \quad (2.9)$$

In reality, D_{AB}/δ and $D_{AB}/\delta(1 - x_A)_{LM}$ are replaced by k_c and k'_c, which are empirically determined mass transfer coefficients (Henley *et al.*, 2011).

2.4 Use of flat sheet membranes for oxygenation of water

The project done by Maynard (2017) focused on the design of a new material or investigating existing materials that would allow the dispersion of micro-bubbles into human blood. The effect of bubbles forming larger bubbles was also investigated.

The test rig used by Maynard (2017) can be seen in Figures 2.5 and 2.6. The setup consists of pressurised oxygen going to a testing chamber, where it is introduced into the water, through a number of flat sheet membranes. Particle image velocimetry (PIV) is used to determine bubble size.

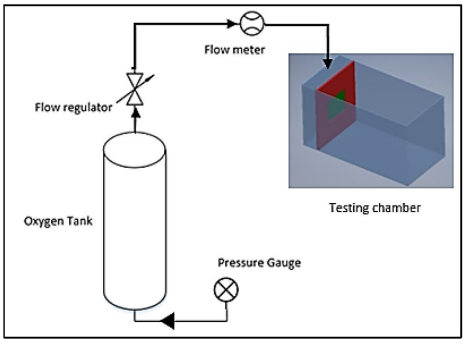

Figure 2.5: Schematic diagram of the experimental setup used by Maynard (2017) to observe bubble formation and behaviour when using different membranes to introduce oxygen into water

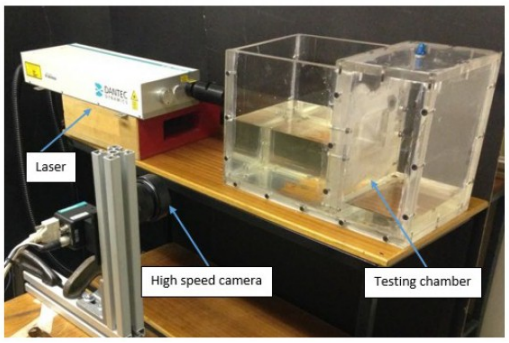

Figure 2.6: Photograph taken showing the experimental setup used by Maynard (2017) to observe bubble formation and behaviour when using different membranes to introduce oxygen into water

Table 2.1: Specifications of the various membranes investigated by Maynard (2017) during experimentation

Material	Pore size
Polytetrafluoroethylene (Teflon, PTFE)	0.2 μm
Polyurethane (tpPUR)	0.6300 μm
Nylon 11 (PA-11)	0.45 μm
Polylactide (PLA)	1 μm
Polyoxymethylene (Acetal,POM)	0.45 μm
Polyglycolic acid (PGA)	5 μm
Polyethylene (PE)	7150 μm

Maynard (2017) investigated a number of possible materials, as listed in Table 2.1, and decided to use Polyurethane mainly due to it's high yield strength. The membranes were tested and it was concluded that micro-bubbles near each other form vortices that disturb the flow of oxygen through the fluid. It was also concluded that these vortices that form were increased as the partial pressure of O_2 was increased. Layering the membrane decreased the flow rate of the oxygen, the deflection of the membrane and the total stress experienced by the membrane. The increased layers also lead to a desired, less volatile, reaction to increased high pressure flow from the oxygen into the fluid. It was stated that PIV is not found to be an accurate method to measure bubble size. The obtained results, Table 2.2, showed that increasing the pressure lead to a decrease in mean bubble size and an increase in dissolved oxygen level (Maynard, 2017).

Table 2.2: Results optained using PIV during experimental testing Maynard (2017)

	1000 Pa	2000 Pa
Oxygen Saturation level [$SaO_2\%$]	5	15
Mean microbubble diameter [μm]	441	403
Dissolution time [ms]	2.5	2.5
Final vulome of oxygen [mL]	10.25	12

2.5 Nano-bubbles

Bubbles with a diameter smaller than 1 μm are classified as nano-bubbles, although typically particles with diameters smaller than 100 nm are classified as "nano" (Chaplin, 2019). The use of nano-bubbles as means of intravascular

oxygenation is suggested as nano-bubbles have a number of properties that make them ideal for this purpose. These properties include a larger contact surface area compared to larger diameter bubbles with the same collective volume, neutral buoyancy, increased gas dissolution rate and a negative surface charge, ensuring bubbles do not combine into larger bubbles.

When considering a fixed volume, the contact surface area is inverse proportional to the radii of the bubbles, for example if the radii of the bubbles decrease by a factor of 10, the total contact surface area is increased by 10. As a greater area of the bubble is exposed to the fluid, in which it is suspended, larger transfer ability is expected (NanoMAX, 2019).

Due to the small size of nano-bubbles they lack sufficient buoyancy to rise to the top of the suspension fluid, rather these nano-bubbles follow Brownian motion, which is an erratic movement. Bubbles remain suspended in the fluid leading to more evenly distributed dissolved gas in the liquid, as these suspended bubbles dissolve (Moleaer, 2019).

Due to the neutrally buoyant nature of nano-bubbles, they act as reserves. As the dissolved oxygen decreases, the suspended bubbles dissolve. According to NanoMAX (2019) and Moleaer (2019) these bubbles can stay suspended in water for months. In research done by Meegoda *et al.* (2018) nano-bubbles were generated in solutions with different *pH* values and the zeta potentials and bubble sizes were measured over time. It was observed that after 1 week, nano-bubbles were still present in the solutions. This can be seen in Figures 2.7 and 2.8.

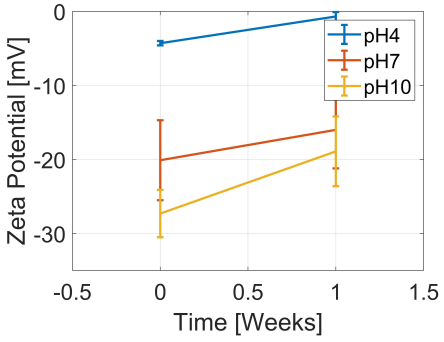

Figure 2.7: Plot of zeta potential of nano-bubbles over time for fluids with different pH values (Meegoda *et al.*, 2018)

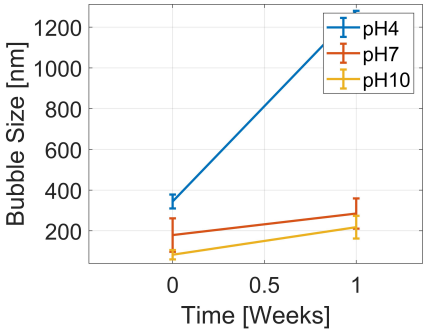

Figure 2.8: Plot of bubble size of nano-bubbles over time for fluids with different pH values (Meegoda *et al.*, 2018)

A key factor to the stability of nano-bubbles is zeta potential (Moleaer, 2019). Nano-bubbles have a negative surface, called zeta potential. Due to this surface charge there is a repulsion force between nano-bubbles ensuring they do not combine to form larger bubbles.

2.6 Generation of nano-bubbles by means of ceramic membranes

In a set of experiments by Ahmed *et al.* (2018), nano-bubbles are generated using tubular ceramic membranes and the effects of pore size, gas inlet pressure and surface coating are investigated. The experimental setup, as seen in Figure 2.9, consists of a compressed gas tank, pressure regulator, gas flow meter, gas filter and tubular ceramic membranes.

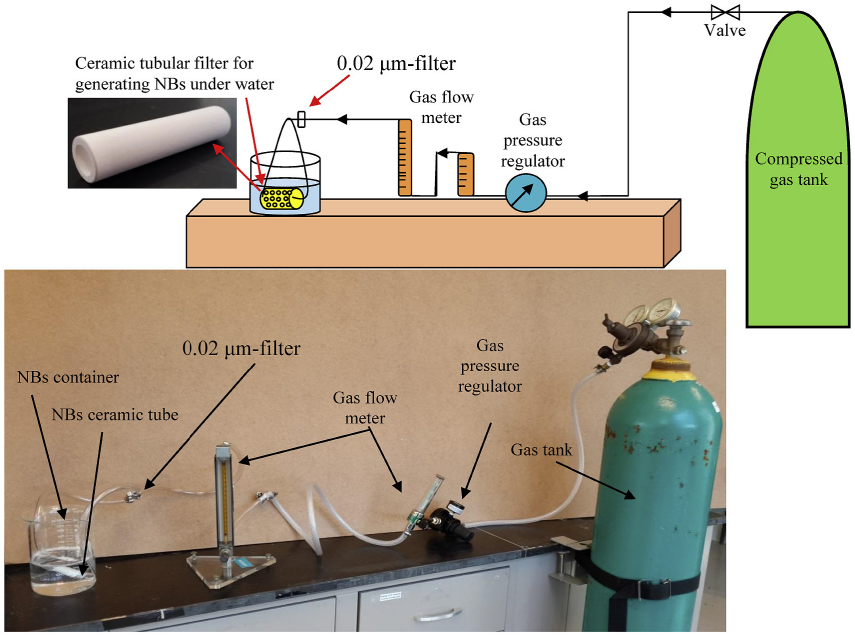

Figure 2.9: A schematic diagram and photo of the experimental setup used by Ahmed *et al.* (2018) to generate nano-bubbles

Two membranes were used with different nominal pore sizes. The two different membranes were manufactured by Refractron in USA (Models WFA0.1 and WFA1), with pore sizes of 100 nm and 1 000 nm respectively. The properties of these membranes, including the nominal pore size and dimensions of the membrane, are given in Table 2.3.

Table 2.3: Dimensions and nominal pore sizes of the respective membranes used in the experimental setup (Ahmed *et al.*, 2018)

	WFA0.1	WFA1
Nominal pore size	100 nm	1 000 nm
Outside diameter	13 mm	21 mm
Inside diameter	8 mm	15 mm
Length	51mm	76 mm

Two of the experiments, done by Ahmed *et al.* (2018), that are of interest for the purposes of this project are the effect of gas inlet pressure on the size of the nano-bubbles and the effect, of the pore size of the membrane, on the bubble size and zeta potential.

To investigate the effect of gas inlet pressure on bubble size, the WFA0.1 membrane was placed in a flask with 500 mL of Milli-Q deionized water and compressed air, oxygen and nitrogen were used to produce nano-bubbles. The compressed air was injected at inlet pressures of 0.69, 1.38, 2.07, 2.75, 3.45 and 4.14 bar. Gas was injection through the membrane for 1.5 $hours$, for each different gas, and measurements of the particle size distribution, zeta potential, pH, dissolved oxygen and temperature were taken. The particle size distribution and zeta potential were measured using a Malvern Instruments Zetasizer Nano ZS.

In Figure 2.10 the plots of mean hydrodynamic diameter, of air nano-bubbles, over time at various inlet pressures can be seen. Ahmed *et al.* (2018) noted that the tendency is for the diameter to decrease over time and concluded this could be due to one of two reasons. The first reason being that initially the passage of air through the membrane is unstable, leading to large variation in bubble size. It is expected that the large bubbles float to the top, due to buoyancy, and leave the water, with the smaller bubbles left in the water. Ahmed *et al.* (2018) continues to state that as time passes the nano-bubbles are retained in the suspension, which explains the declining trend in bubble size. The second reason presented is that the large surface tension of the nano-bubbles and constant gas exchange at the interface between the surface of the nano-bubble and the water, causes the size of the bubbles to decline and stabilize.

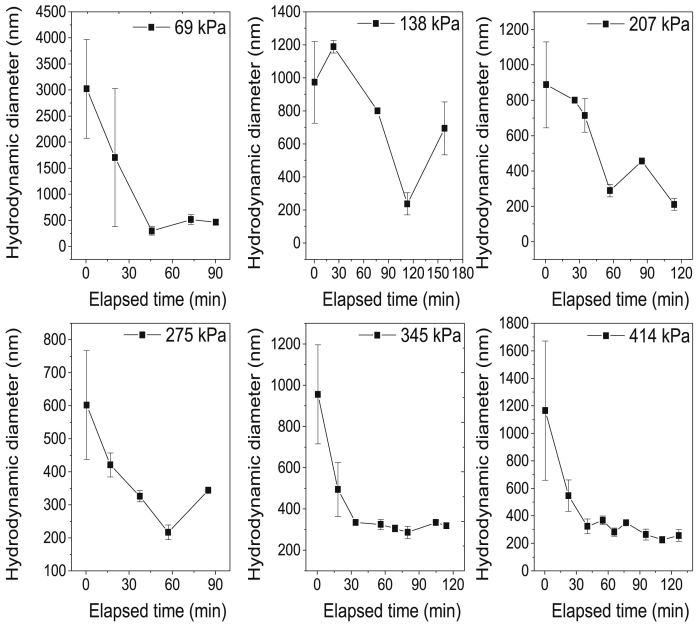

Figure 2.10: Plots of hydrodynamic diameter over time of air nano-bubbles at different inlet pressures (Ahmed *et al.*, 2018)

In Figure 2.11 plots, at different pressures, of zeta potential over time are given. It was stated by Ahmed *et al.* (2018) that the zeta potential decreases over time and is unstable at 69, 138 and 207 kPa and that the zeta potential stabilises at between -25 and -30 mV after 30 min when the pressure is at 414 kPa.

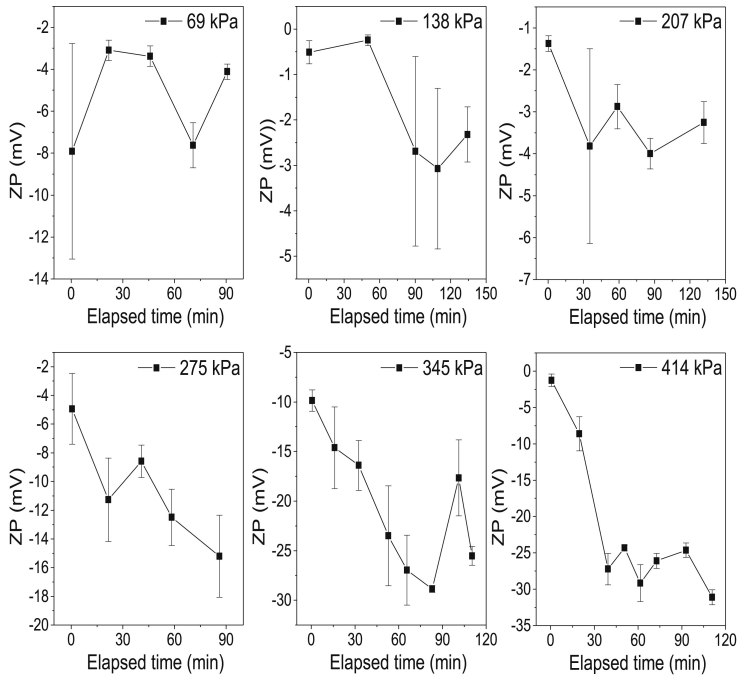

Figure 2.11: Plots of zeta potential over time of air nano-bubbles at different inlet pressures (Ahmed *et al.*, 2018)

The zeta potential is significantly lower at 414 kPa. Ahmed *et al.* (2018) attributes this to the reduced bubble size at higher inlet gas pressures. The same tendency, of declining zeta potential, was observed when using nitrogen and oxygen to generate nano-bubbles. The zeta potential at 414 kPa of the oxygen and nitrogen nano-bubbles were -38 mV and -45 mV respectively. As can be seen these values of the different gasses differ and is attributed to the different properties of the gasses with regard to surface absorption of ions, surface ionization energies or polarity.

The change in the dissolved oxygen level, as oxygen nano-bubbles are injected into the water over time, can be seen in Figure 2.12. It was observed that the dissolved oxygen level increases for the first 10 minutes, after which it reached a plateau. An increase in temperature of the water was observed over time.

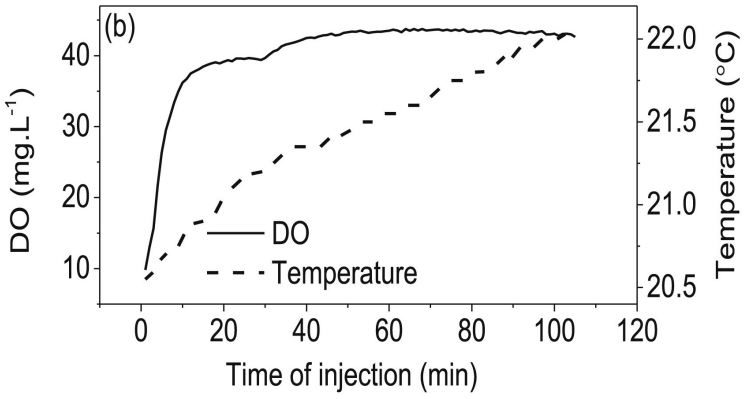

Figure 2.12: Plot indicating the change in the dissolved oxygen level as oxygen is injected into the water over time (Ahmed *et al.*, 2018)

Air was injected at 4.14 *bar* into the 500 *mL* water. The two different membranes, as seen in Table 2.3, were used to determine if pore size affects bubble size and zeta potential. In Figures 2.13 and 2.14 the particle size distribution and zeta potential measurements of nano-bubbles generated using a 100 *nm* and 1000 *nm* membrane can be seen.

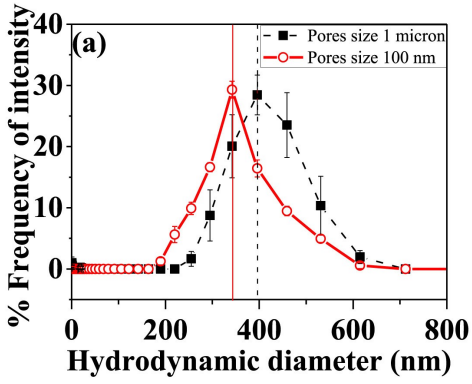

Figure 2.13: Particle size distribution measured of air nano-bubbles that were generated using two different membranes with a 100 *nm* and 1000 *nm* nominal pore size (Ahmed *et al.*, 2018).

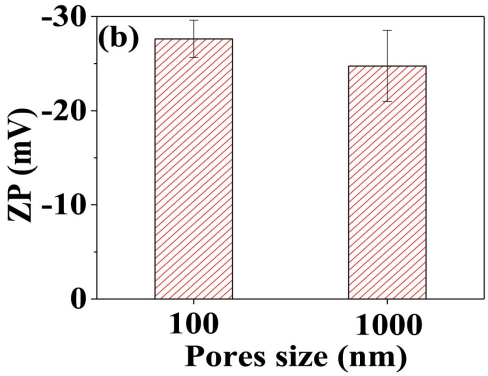

Figure 2.14: Zeta potential (ZP) measurements of air nano-bubbles that were generated using two different membranes, one with a 100 *nm* and a 1000 *nm* nominal pore size (Ahmed *et al.*, 2018).

Ahmed *et al.* (2018) noticed that the hydrodynamic diameters fell between 200 *nm* and 650 *nm*, peaking at 340 *nm* and 390 *nm* for the membranes with

pore sizes 100 nm and 1 000 nm, respectively. It was predicted that the pore size will affect the bubble size by 10 times. Ahmed *et al.* (2018) concluded that the bubble size is affected by the nominal pore size of the membrane, but not by 10 times, as predicted. The bubble sizes not conforming to the predicted difference was attributed to the differing flow rates of 0.45 $L \cdot min^{-1}$ and 15 $L \cdot min^{-1}$, through the 100 nm and 1 000 nm membranes, respectively. Ahmed *et al.* (2018) observed that the zeta potential is slightly less negative for the nano-bubbles generated using the membrane with the 1 000 nm pore size than the bubbles generated using the membrane with the 100 nm pore size.

2.7 Conclusion: Literature review

A literature study was conducted, meeting Objective 1. The function of the pulmonary system was investigated and it was determined that the global oxygen consumption of a healthy 75 kg human is 250 mL/min. It was determined that the amount of oxygen delivered in the body is greatly affected by the amount of haemoglobin in the blood as well as the cardiac output. The average cardiac index was investigated and it was determined to be at an average of 3.1 $L/min/m^2$ for women and 3.2 $L/min/m^2$ for men.

Known blood oxygenation methods, including ECMO and IVOX were discussed. ECMO is an intricate system and a high cost is associated with treatment using ECMO. IVOX was discovered to only supply 25% of the basic oxygen requirements of a human. The use of IVOX also include a number of risks, some of which are fatal.

Mass transfer from a gas to a liquid was investigated and it was determined that steady state diffusion is dependent on the concentration gradient and the contact surface area. According to the film theory a liquid film exists where diffusion has already started to occur. This film has a higher concentration of gas than the bulk liquid, but lower concentration than the gas. The gas must diffuse through this layer and due to the smaller concentration gradient it acts as a "resistance" between the gas and the bulk liquid.

In a project done by Maynard (2017) membranes were used to generate oxygen bubbles in water. The membrane used had a pore size of 0.630 nm and the bubbles generated were determined to have mean pore size of 441 μm when a oxygen pressure of 1000 Pa is used and 441 μm at a pressure of 2000 Pa. From this it was concluded that to generate nano-scale bubbles membranes with smaller pore sizes should be considered and the effect of higher pressures should be investigated.

Nano bubbles have a number of properties that could be beneficial when used in oxygenation. These properties were investigated. These properties include a larger contact surface area compared to larger diameter bubbles with the same collective volume, neutral buoyancy, increased gas dissolution rate and a negative surface charge, ensuring bubbles do not combine into larger bubbles.

An set of experiments were done by Ahmed *et al.* (2018), using tubular ceramic membranes. The membranes used had pore sizes of 100 nm and 1 000 nm. From the experiments it was determined that the size of the bubble generated does depend on the pore size, but the difference in bubble size is not of the same magnitude than the difference in pore size. Bubbles generated using the 100 nm and 1 000 nm had mean diameters of 340 nm and 390 nm, respectively.

The experiments done by Maynard (2017) and Ahmed *et al.* (2018), both use a membrane to oxygenate water that is static and in a container that is open to atmosphere. As the water is static on the membrane a shear force caused by the water flowing over the membrane is not applicable. For the purposes of this project it is important to determine the oxygenation of water flowing over the membrane at a flow rate mimicking the flow rate of blood.

As the containment area of the water is open to atmosphere for both of these experiments, it is possible for large oxygen bubbles to rise to the top and escape the water. This is problematic for the purposes of this project as the detection of large bubbles forming is critical. Another factor influenced by the fact that the water is in an open container is the pressure of the water. As the water level is quite low, the hydrostatic pressure is relatively small. To mimic the blood pressure the hydrostatic pressure should be at 1.6 mH_2O. This is important as the pressure difference is expected to affect the oxygen transfer and dissolution.

Chapter 3

Design of Experiments

In Chapter 2 a literature study was conducted to gain valuable background information regarding the pulmonary system, known oxygenation methods, previous research regarding intravascular oxygenation and the properties of nano-bubbles. In this chapter the design of the experimental setup is discussed. The system is discussed as a whole and the detail designs are given.

This chapter discusses the experimental setup and the design and purpose of the individual components as well as the experimental procedure.

The experiment is designed to mimic the human pulmonary system as closely as possible, while using water as the working fluid. The important factors that are mimicked include the volume flow rate, the piping diameter and the pressure. These factors are discussed in this chapter.

An experimental setup is designed to introduce nano-scale oxygen bubbles into water and measure the properties of these oxygen bubbles. The setup consists of a number of components that work together. Each component is discussed in terms of purpose and design. The main design feature of the experimental setup is the inlet manifold where oxygen is introduced into the water, through a membrane. Two different designs of the inlet manifold were used during experimentation and both are described in this chapter.

For the first design of the inlet manifold, flat sheet membranes were used and for the second design, tubular membranes were used. The properties of these membranes are discussed in Chapter 4.

A number of digital design tools are available and give engineers a great advantage as detailed 3D designs can be made and analysed before manufacturing commences. This chapter highlights these design tools that were used during the design process. These tools include the CAD package, Autodesk Inventor,

which was used to design both iterations of the inlet manifold as well as the buffer tank.

3.1 Response surface methodology

Response surface methodology is used to design the experiments. This consists of selecting the values for the variables using the Box-Behnken method, as discussed in Chapter 5, conducting the experiments, fitting a surface to the data and then analysing the variance as well as determining the goodness of fit of the surface to the data. The surface is then optimised to determine in which region the expected near-optimum is. The entire process is then repeated by selecting variables within this new range where the expected near-optimum is.

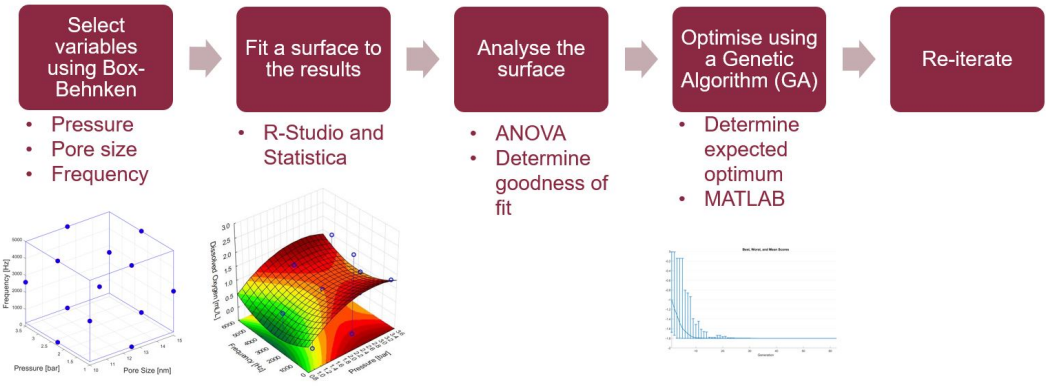

Figure 3.1: The individual steps involved in response surface methodology, which is the method used to design the experiments

The independent variables are pressure, pore size and frequency and the dependent variables are dissolved oxygen and bubble size. R-Studio is used to fit a function to the data and this fitted function/surface is analysed using analysis of variance (ANOVA) to determine the significance of each variable. The R^2 value is determined to analyse how well the function represents the data. A genetic algorithm (GA) is used to determine the near optimum of the function.

GA's are inspired by natural selection, where the fittest/strongest individuals survive and reproduce to create the next generation (Mallawaarachchi, 2020). The algorithm starts off by generating a random initial population of individuals consisting of different combinations of the three independent variables. A fitness value is determined for each individual in the current generation and the

fittest/strongest individuals are used to create the following generation. Children are produced by making random changes to a parent, called mutation, or by combining properties of two parents, called cross-over (Mathworks.com, 2020).

3.2 Experimental Setup

The experimental setup is designed to mimic certain aspects of blood flow in the human body, such as pressure and flowrate.The main components are the inlet manifold, the buffer tank and the dissolved oxygen probe. The components are connected using PVC piping and the valves and instrumentation units aid in controlling flow and measuring pressure and temperature.

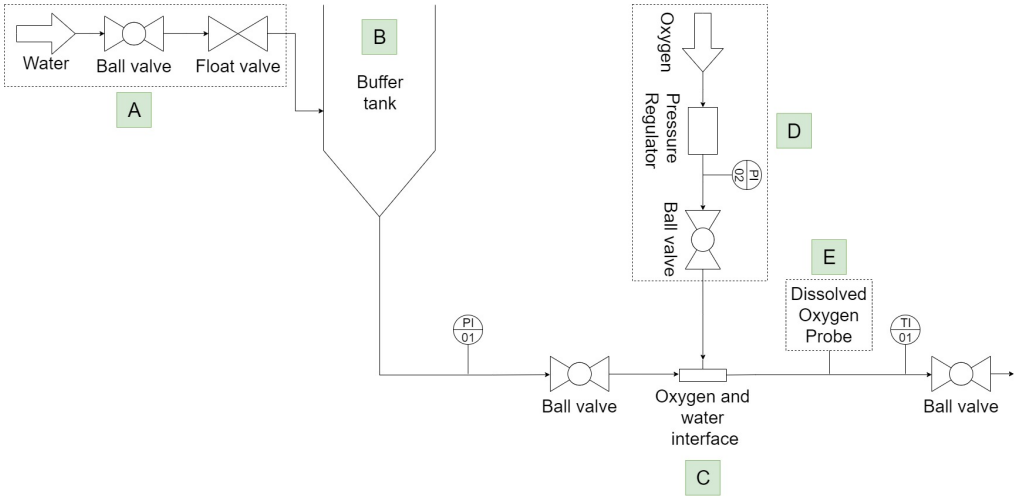

Figure 3.2: Schematic diagram of experimental setup showing water flow control (A), buffer tank (B), oxygen and water interface (C), oxygen inlet and flow control (D) and dissolved oxygen probe (E)

It can be seen in Figure 3.2 that Reverse Osmosis (RO) water is supplied to the system through a main shut-off valve after which it enters the buffer tank, indicated as component B, through a float valve. RO water is used to ensure that the water going through the system is free of debris, as debris and other impurities in the water could potentially clog the pores of the membranes and affect readings. RO water is also free of dissolved salts, which could affect oxygen solubility.

The buffer tank is used to ensure a constant flow of water to the system despite possible variations in the inlet flow rate. The buffer tank also serves

as pressure control due to the fact that it is installed at a fixed height, 1.6m above the inlet manifold, that mimics the average systolic blood pressure of 120 $mmHg$. The float valve, as can be seen in Figure 3.3, is used to maintain a constant water level in the buffer tank and it ensures that the buffer tank does not overflow. The buffer tank is vented to atmosphere to ensure that the water in the tank can freely flow without causing a vacuum.

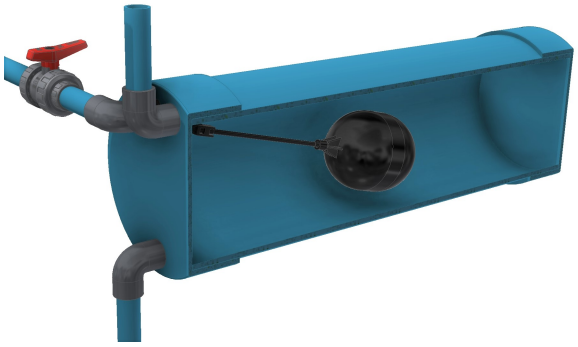

Figure 3.3: A 3D Rendering of the buffer tank assembly, as drawn using Autodesk Inventor, with the inlet connected to a float valve which ensures a constant water level in the tank.

The buffer tank outlet is connected to the oxygen inlet manifold through a ball valve. The oxygen inlet manifold, component C in Figure 3.2, is used to introduce oxygen through a membrane into the passing water. Two different designs for the inlet manifold are discussed in Sections 3.3 and 3.4. A pressurised oxygen tank is used to introduce oxygen (99.5% purity) into the system. The experiment requires that oxygen enters the inlet manifold at different pressures and this is controlled using the pressure regulator.

A Mettler Toledo, membrane type, dissolved oxygen (DO) probe connected to a Mettler Toledo M300 transmitter is used to measure the level of dissolved oxygen in the water as well as the temperature of the water. The DO probe is installed 300 mm from the inlet manifold.

3.3 Inlet manifold using flat sheet membranes

The inlet manifold is a key component of the experimental setup as it used to introduce oxygen into the water, through a membrane. The design thereof is

discussed in this section and the strengths and weaknesses of the two different designs are compared.

3.3.1 Working principle of the inlet manifold using a flat sheet membrane

A set of flat sheet membranes, as discussed in Sections 4.1 and 4.2, were used in this setup. The membrane was mounted between two flanges and sealed using silicon gaskets. The membrane serves as an interface, with water passing by on the one side and pressurised oxygen on the other side. The purpose of this is to allow the oxygen to permeate the membrane and enter into the water.

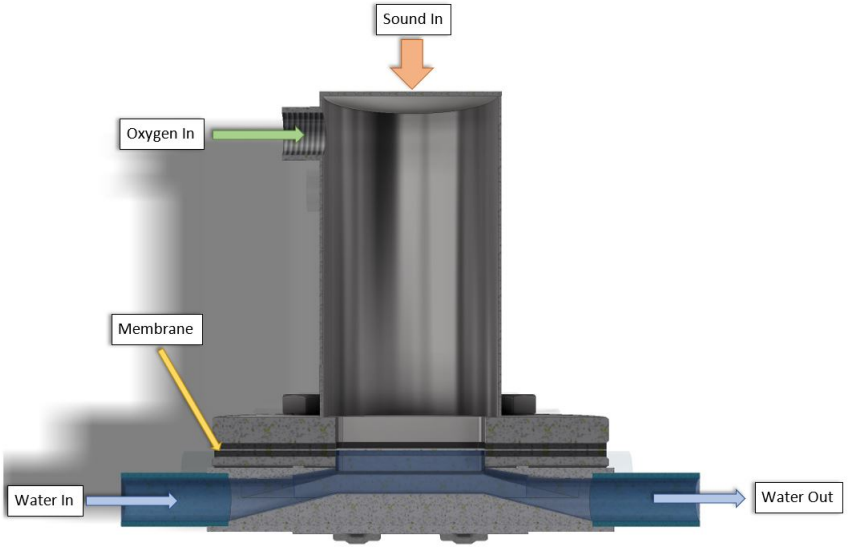

Figure 3.4: Sectional view of the inlet manifold assembly with the flat sheet membrane mounted between the two flanges.

As illustrated in Figure 3.4, oxygen enters the pressure vessel at the top of the inlet manifold. A 5 $Watt$ speaker is mounted to the top of the pressure vessel in order for the system to be vibrated at various frequencies.
The throat section, where the water flows through, is designed to have a constant hydraulic diameter to ensure that the water passing through makes contact with the membrane and that there is no sudden expansion in the throat. The total contact area of the membrane is 14 cm^2.

3.3.2 Inlet manifold design for a setup using a flat sheet membrane

The inlet manifold is designed as two separate parts, a 3D printed inlet tube and a stainless steel flange. The 3D printed inlet tube is designed to fit onto a PVC pipe with a inner diameter (ID) of 20 *mm* and an outer diameter (OD) of 25 *mm*. It has a slot on the top where a gasket is fitted to ensure that the flange seals on the inlet tube. The flange is designed according to the dimensions of a NB65 1000/8T12 flange. As seen in Figure 3.5 the 3D printed part is mounted to the flange using pipe clamps and M6 stainless steel bolts and nuts. The pipe clamps have soft rubber linings to ensure that the 3D printed inlet tube is not damaged. Great care should be taken when tightening the M6 nuts and bolts, as over-tightening it could damage the inlet tube.

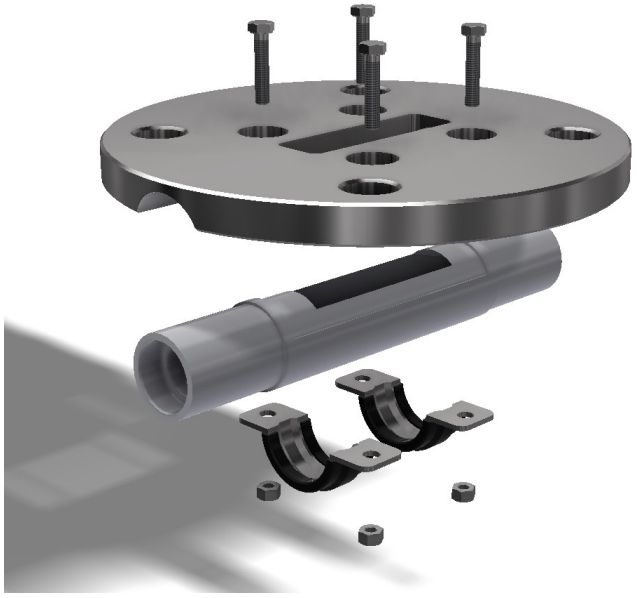

Figure 3.5: A rendering of the inlet manifold assembly. The assembly consists of a 3D printed inlet tube and a stainless steel flange fitted together using pipe clamps

Figure 3.5 illustrates that there is a rectangular opening through the flange. This is the area where the oxygen goes through the membrane into the water. The 3D printed inlet tube is designed in such a way that there is a smooth transition from the rectangular opening, at the top of the part, to the pipe diameter. This is done to reduce the chance of turbulent eddies forming, due to sudden expansion, across the membrane and also to improve water-membrane contact.

3.3.3 Design of the pressure vessel for the inlet manifold

A pressure vessel is designed to evenly distribute the oxygen over the membrane. It is also where the speaker is mounted to vibrate the membrane. The vessel is designed according to SANS 347-2012, as discussed in Appendix B. It is designed using standard size NW80 dairy tube, capable of 15 *bar* pressure, with stainless steel end caps welded on. The oxygen inlet of the vessel is a standard 1/4" BSP socket, that is welded into the side of the tank. A high pressure, press-in, pneumatic fitting is used to connect the line from the oxygen tank to the pressure vessel.

Figure 3.6: Exploded views of the inlet manifold assembly,at different angles, showing the oxygen inlet pressure vessel, the silicon gaskets, the 3D printed inlet tube and the required fasteners

Before the pressure vessel is used, it is pressure tested, to ensure that there are no leaks and that the vessel can maintain the desired pressure. The pressure vessel is mounted to the inlet manifold assembly, as seen in Figure 3.6. The membrane is mounted between two gaskets and placed between the flanges of the pressure vessel and the inlet manifold. This assembly is fastened using M16, stainless steel, bolts and nuts.

3.4 Inlet manifold using tubular ceramic membranes

One of the advantages of using response surface methodology, which consists of multiple experimental runs, is that there is room for continuous improvement of the physical setup. Due to the shortcomings of the first iteration membranes a new design is required.

During experimentation using the inlet manifold with the flat sheet membranes, large bubbles were observed and it was concluded that the water does not make sufficient contact with the membrane. This is discussed in detail in Chapter 5.

The new design uses tubular ceramic membranes, as discussed in Section 4.2. The design of the inlet manifold, using tubular ceramic membranes, and the advantages of using these membranes are discussed in this section.

3.4.1 Working principle of the inlet manifold using a tubular ceramic membrane

The purpose of the design is to introduce nano-scale oxygen bubbles into water. Oxygen enters the inlet manifold through the pressure vessel and then permeates the ceramic membrane into the water. The water flows over the outer surface of the ceramic membrane as can be seen in Figure 3.7. Sound is introduced through the top of the pressure vessel, by means of a speaker that is mounted to it. This is done to vibrate the system at various frequencies.

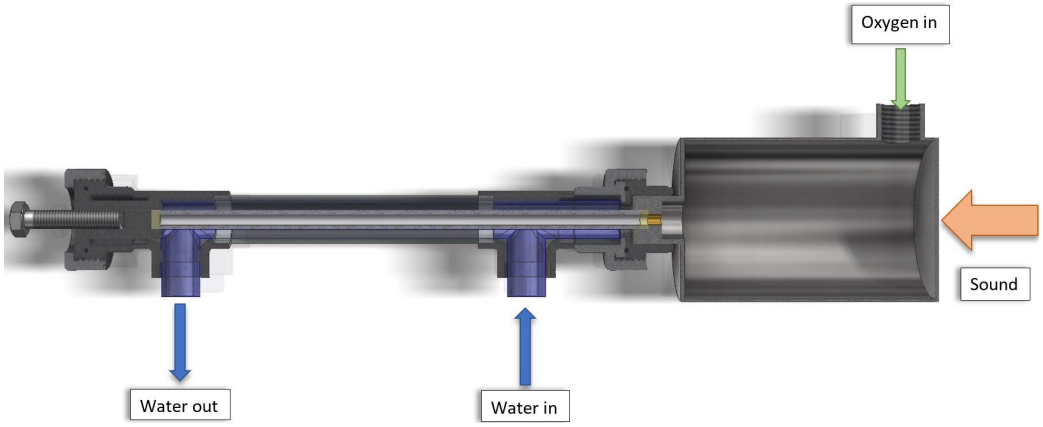

Figure 3.7: Sectional view of the inlet manifold, using a ceramic membrane, indicating water and oxygen flow in the experimental setup

Advantages of this design is that there is a larger contact area of 50 cm^2 between the membrane and the water. Perspex tubing is used at the interface between the water and the membrane, which gives the advantage of being able to see what happens on the membrane surface making it possible to detect any large bubbles forming.

3.4.2 Inlet manifold design for a setup using a tubular ceramic membrane

The membrane is mounted in a transparent Perspex tube, with a water inlet and outlet consisting of standard PVC T-pieces. The membrane is sealed on the edges using custom made silicon gaskets. The air inlet side is connected to the inlet pressure vessel, where the inlet oxygen is vibrated at various frequencies using a speaker. The other end of the membrane is blanked off. The mounting space for the membrane is adjustable, ensuring that the different membranes will seal.

Figure 3.8: Exploded view of the revised design of the inlet manifold assembly consisting of the pressure vessel, membrane housing and membrane

As can be seen in Figure 3.8, the inlet manifold is constructed using standard

PVC fittings, such as unions and T-pieces. The unions are used to dissemble the pressure vessel side as well as the adjustable side.

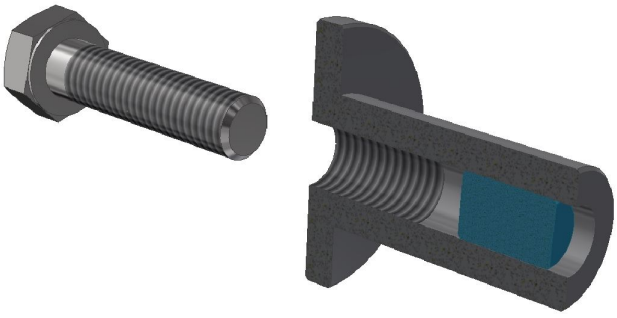

Figure 3.9: Exploded view of the adjustable section of the inlet manifold.

Figure 3.9 shows the adjustable section consisting of a machined PVC housing, with internal thread, a stainless steel bolt and a slider. As the bolt is tightened the slider moves forward, sealing the membrane. This is required as different membranes have small variations in length. Great care should be taken not to over-tighten the membrane, as this could damage it.

3.4.3 Pressure vessel for the second generation design

The inlet pressure vessel that is used in the inlet manifold that was designed for the flat sheet membranes is re-used. The flange is cut off and a stainless steel end cap is welded on. A machined stainless steel stub, with thread on the outside, is welded onto the bottom of the tank, and serves as the inlet mounting for the membrane.

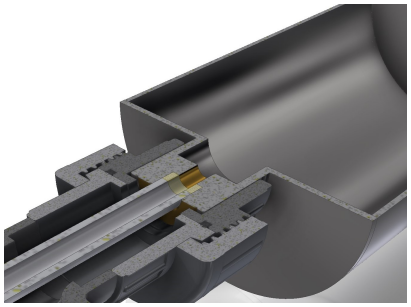

Figure 3.10: Pressure vessel mounted to the inlet assembly

3.5 Experimental method

To ensure accurate results the appropriate experimental method should be determined. Calibration of measuring equipment is of the utmost importance as well as the methodology for obtaining the required measurements.

3.5.1 Oxygen probe calibration and measurements

Before every set of experiments the dissolved oxygen probe is taken out of the system, dried and recalibrated in atmospheric air. This is done in accordance with the manufacturer's calibration procedure. It is assumed that air contains 20.9% oxygen. After the meter is calibrated it is inserted back into the system.

3.5.2 Important zero-readings

Before experiments are conducted the system flow rate is adjusted, by throttling outlet ball valve. The correct flow rate is determined by timing the flow into a measuring cup and throttling accordingly.

A critical zero reading that should be recorded is the zero reading of the water. This is done to determine the amount of dissolved oxygen in the water when no additional oxygen is added. This is done before every set of experimental runs to ensure accuracy.

3.5.3 Experimental procedure

The first step is to mount the membrane that is to be used for the experiment. It is important to ensure that the ball valve at the bottom of the buffer tank, before the inlet manifold, is closed. After the desired membrane is mounted, the water inlet is connected and opened. The water is left to run until the float valve in the buffer tank closes.

It is important to ensure the pressure regulator is set to 0 *bar* before beginning. The ball valve at the bottom of the buffer tank is opened and the water is left to run for 5 *minutes* in order for the dissolved oxygen probe to measure the water zero-reading for that specific run. After the 5 *minutes* have passed, the oxygen cylinder is opened and the regulator is adjusted to the desired pressure. Dissolved oxygen readings are recorded and after 10 *minutes* the oxygen tank valve is closed and the regulator turned back to zero. The ball valve below the buffer tank is closed and the water in the piping is drained to remove any

oxygenated water from the system. This procedure is repeated three times for every combination of variables.

3.5.4 Particle size and zeta potential determination

An Anton Paar Litesizer^{TM} is used to measure the particle size and the zeta potential. Samples are taken from a sampling point located after the inlet manifold. Samples are taken through a small tube located in the middle of the larger tube.

Firstly a sample is taken out of the tube into a 500 mL flask. Care should be taken not to agitate the mixture, as this might affect the properties of the nano-bubbles. A syringe is used to carefully extract a sample and put it in a cuvette. A cuvette is a small tube like container that is placed in the Anton Paar Litesizer^{TM} to measure particle size. The refractive index is set to 1 (Ahmed *et al.*, 2018), to determine bubble size, and the data is recorded. This entire process is repeated three times.

To determine the zeta potential the samples are also collected in a flask and extracted using a syringe, but then it is placed in a special cell that is also inserted into the Anton Paar Litesizer^{TM} . The zeta potential readings are repeated three times for every setup and recorded.

3.6 Conclusion: Design of experiment

The experiment is designed to mimic the human pulmonary system as closely as possible with regards to pressure, pipe diameter and volume flow rate.

The design of the experimental setup is discussed, focussing on the various components and the function of each. Two different inlet manifolds, using flat sheet membranes and tubular ceramic membranes, are discussed.

Chapter 4 discusses the membrane specifications as well as the methods used to validate it.

Chapter 4

Membrane specifications

As discussen in Chapter 3, membranes are used to introduce oxygen into water. The oxygen permeates the membrane and enters the water flowing over the membrane. It is aimed to form nano-scale oxygen bubbles in the water. As discussed in Chapter 2, it was stated by Ahmed *et al.* (2018), that gas nano-bubbles can be generated in water using membranes and that the size of the bubbles depend on the pore size of the membrane.

For the experiments two different types of membranes are used, namely flat sheet membranes and tubular membranes. This chapter covers the various membranes used in the experimental setup, discussing membrane properties such as pore size and material. Membrane specifications are verified and the verification method and results are discussed. The motivation for the membrane pore size selection is discussed in Chapter 5.

4.1 Flat sheet membranes

Flat sheet membranes are typically used in filtration applications. For the purposes of this project membranes are used with the aim to generate oxygen nano-bubbles in water. To ensure accuracy, membrane specifications are validated.

4.1.1 Flat sheet membrane specifications

Flat sheet membranes are used for the first experimental designs. The membrane pore sizes were selected based on the Box-Behnken design method, as discussed in Chapter 5. Another consideration was the cost of the membrane as well as availability.

The desired membrane range was selected as between 50 nm and 10 nm. The supplier had a number of membranes available within that range and the following membranes, as seen in Table 4.1, were selected.

As seen in Table 4.1 the specifications include Molecular Weight Cut-Off (MWCO). MWCO is used to describe the permeability of a membrane and is defined on the basis of 90% rejection of particles of a specific molecular weight (Scott, 2006).

Table 4.1: Specifications of sourced membranes as given by suppliers, showing membrane chemistry and Molecular Weight Cut-off or nominal pore size

Membrane	Membrane Chemistry	Molecular Weight Cut-Off (MWCO)
TRISEP® UB70	Polyvinylidene Fluoride (PVDF)	0.03 μm (nominal pore size)
SelRO® MPS-34	Propriety composite	200 000 Dalton
NADIR® UH050 P	Hydrophilic Polyethersulfone (PESH)	50 000 Dalton
NADIR® UH010 P	Polyethersulfone (PES)	10 000 Dalton

MWCO over nominal pore size is represented by a logarithmic function as seen in Figure 4.1. This is used to convert between MWCO and nominal pore size in nano-meter (nm).

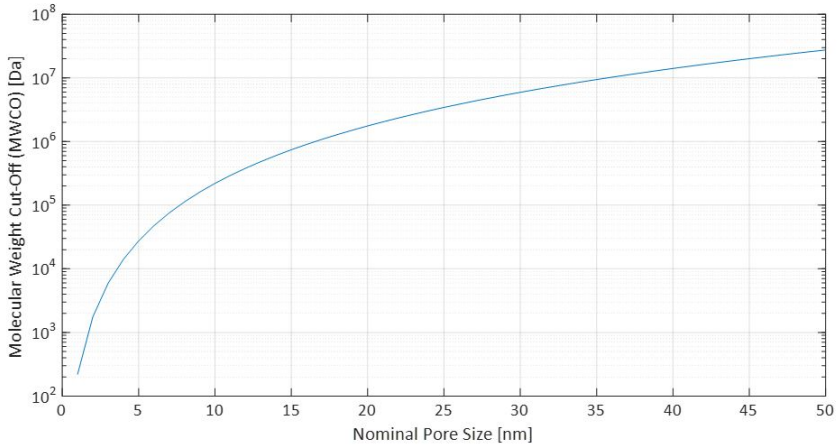

Figure 4.1: Plot of Molecular Weight Cut-off vs Nominal Pore Size in nanometer generated using MATLAB (2019)

4.1.2 Verification of membrane pore size

The nominal pore size of the membrane has an significant effect on the size of the nano-bubbles (Ahmed *et al.*, 2018). To ensure accurate experimental data it is important to verify the actual pore size. This was done using image analysis and comparing the results to the specifications as given by the suppliers.

A Scanning Electron Microscope (SEM) was used to take images of the supplied membranes. This entails cutting off a small sample of the sheet membrane and sticking it to sample pin, that is inserted in the SEM. The images of the respective membranes are shown in Figure 4.2 to Figure 4.5. Larger images are available in Appendix C. In the bottom left corner the scale of each image can be seen.

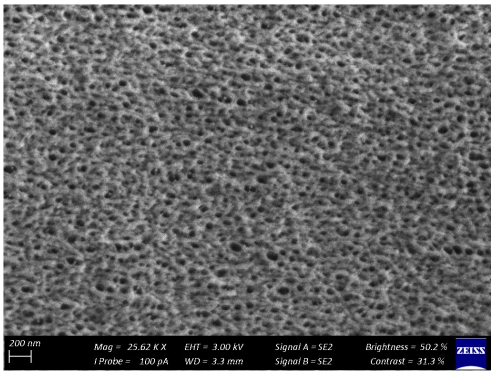

Figure 4.2: Scanning electron microscope image of TRISEP® UB70

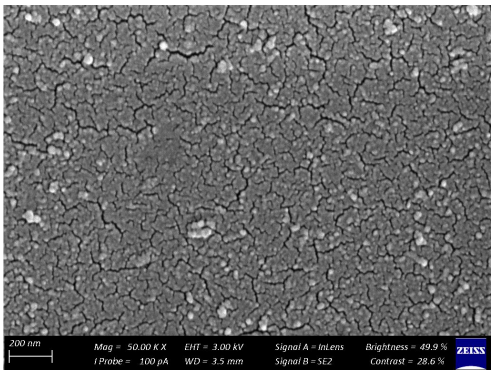

Figure 4.3: Scanning electron microscope image of SelRO® MPS-34

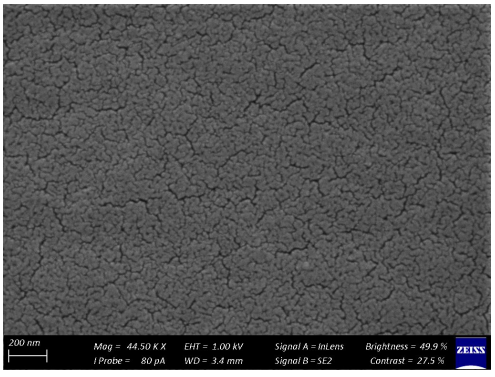

Figure 4.4: Scanning electron microscope image of NADIR® UH050 P

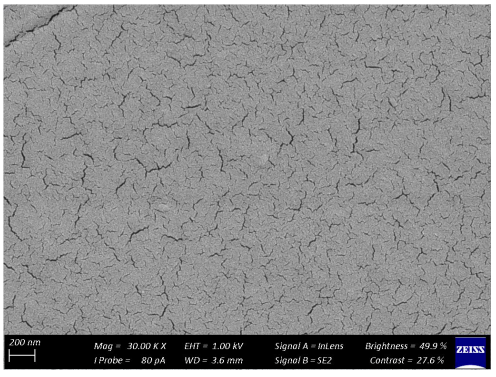

Figure 4.5: Scanning electron microscope image of NADIR® UH010 P

The TRISEP® UB70 membrane, as seen in Figure 4.2, has elliptically shaped pores whereas the SelRO® MPS-34, NADIR® UH050 P and NADIR® UH010 P membranes have pores resembling cracks, as seen in Figure 4.3 to 4.5.

It was expected that all the membranes had spherical pores, simular to the TRISEP® UB70. Molecular weight cut-off is used to describe the nominal pore size distribution and the filtering capabilities of a membrane. It describes the lowest molecular weight, measured in daltons, at which more than 90% of the solute is retained by the membrane (Synderfiltration, 2019). It is concluded that the membranes are rated according to their retaining capability and that the pores are not necessarily spherical. The membrane cracks are thin enough to retain particles larger than the rated MWCO.

Image analysis is done, using ImageJ software, to determine the nominal pore size of each membrane. This is done by determining the average area of the pores or cracks and then converting these areas to hydraulic diameter.

Table 4.2: Comparison of expected and actual pore size

Membrane	Expected nominal pore size	Actual nominal pore size
TRISEP® UB70	30 nm	30 nm
SelRO® MPS-34	10 nm	15 nm
NADIR® UH050 P	4 nm	12.5 nm
NADIR® UH010 P	2.5 nm	10 nm

Table 4.2 compares the expected and actual pore size, as determined using image analysis. The actual pore size of the TRISEP® UB70 membrane is the same as the expected pore size, whereas the actual pore size of the SelRO® MPS-34, NADIR® UH050 P and NADIR® UH010 P membranes differ from the expected pore size. The hydraulic diameter does not correspond to the expected pore size, as the membranes do not have spherical pores, but rather cracks. Although these cracks contain particles larger than a certain diameter, the area of the crack is larger, leading to a larger hydraulic diameter.

Possible implications of the membranes having cracks rather than elliptical pores are that larger bubbles can form through the crack than would through

a pore. When the membranes are used in filtration applications solid particles larger than the width of the crack cannot permeate the membrane, but oxygen can permeate the entire crack, forming a larger bubble on the water side. Figure 4.6 is an illustration of this.

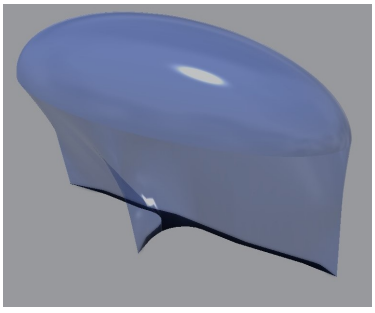

Figure 4.6: Illustration of a gas bubble forming through a crack

4.2 Tubular ceramic membranes

Tubular ceramic membranes were used, similar to those used in experiments done by Ahmed *et al.* (2018). In this section the properties of these membranes are discussed.

4.2.1 Tubular ceramic membrane specifications

In Table 4.3 the specifications of the tubular ceramic membranes are given. All the membranes come from the same supplier and are the same type of membrane with regards to material, shape and dimensions. The only difference between the membranes is the pore size. Ceramic membranes are typically used for ultra- or nano-filtration applications. Image analysis is not done on the tubular membranes as using the SEM requires a sample, which would require that the membrane be destructed.

Table 4.3: Specifications of the tubular ceramic membranes

Membrane	Material	Pore Size	Diameter	Length
Type 6/10-250	Al2O3/TiO2	50 nm	10 mm	200 mm
Type 6/10-250	Al2O3/TiO2	100 nm	10 mm	200 mm
Type 6/10-250	Al2O3/TiO2	200 nm	10 mm	200 mm

4.3 Conclusion: Membrane specifications

Two different types of membranes were used during experimentation. The pore size of the flat sheet membranes were validated using a scanning electron microscope and it was concluded that the actual pore shape is different than expected. It was expected that the membranes have elliptical pores, however, it was determined that the SelRO® MPS-34, NADIR® UH050 P and NADIR® UH010 P membranes have pores resembling cracks. This was attributed to the fact that the purpose of these membranes, in industry, is to filter solid particles out of a fluid. As these solid particles are prohibited by the width of the crack, these membranes are sufficient. For gas, however, the length of the crack could affect the bubble size.

In this chapter the properties of the tubular ceramic membranes, that were selected, were discussed. When comparing the properties of the flat sheet membranes to the tubular ceramic membranes it can be seen that the pore sizes of the ceramic membranes are significantly larger.

Chapter 5

Results

In Chapter 3 the experimental setup that was designed and built is described. Two different membranes were used, namely, flat sheet membranes and tubular ceramic membranes. These two types of membranes that are used to conduct the experiments are described in Chapter 4.

This chapter focusses on the results of the experiments, the analysis thereof and determining the near optimum combination of values for the independent variables. The method of initially selecting the values of the independent variables for the experiments is also discussed.

The Box-Behnken design method is used to determine the different sets of values for the three independent variables, namely, the nominal pore size of the membrane, the oxygen inlet pressure and the frequency of the sound wave used to vibrate the inlet oxygen and membrane. The selected ranges for the variables, as used in the Box-Behnken design, are given and discussed.

The results gained from the experiments are tabulated and discussed. A function is fit to the data and analysed using analysis of variance (ANOVA). A genetic algorithm is used to to determine the near optimum of the function.

5.1 Generating bubbles using flat sheet membranes

The first iteration of the experiments used flat sheet membranes with differing nominal pore sizes. Box-Behnken design was used to determine the sets of experiments that need to be conducted and the results of these experiments are given. For these experiments the dissolved oxygen (DO_2), the mean bubble size and the zeta potential, as discussed in Section 2.5, are measured.

5.1.1 Box-Behnken design for experimental variable selection

Box-Behnken is an efficient method by which the different combinations of variables are selected. The Box-Behnken design method requires fewer runs than a normal factorial technique, but still has enough data points to fit a representative surface in the selected area. The ranges for the variables can be seen in Table 5.1 below.

Table 5.1: The ranges of the variables as used in Box-Behnken

Variable	Minimum Value	Maximum Value
Pore Size	10 nm	15 nm
Pressure	1 bar	3.5 bar
Frequency	200 Hz	5 000 Hz

The initial selected range of the nominal membrane pore size was selected as 2.5 nm to 30 nm. In experiments done by Maynard (2017), as discussed in Section 2.4, flat sheet membranes with a pore size of 0.63 μm were used to generate bubbles in water. This resulted in bubbles with a average bubble size of 441 μm and 403 μm at pressures of 1 000 Pa and 2 000 Pa, respectively (Maynard, 2017). As these bubbles are too large (not nano-scale), the nominal membrane pore size was selected to be significantly smaller and the pressure higher.

As discussed in Chapter 4, the actual nominal pore size differs from the expected values and therefore the selected range is 10 nm to 15 nm. The membrane with the 30 nm nominal pore size fractured, as can be seen in Figure 5.1, at a pressure of just over 4 bar, therefore the selected pressure range is from 1 bar to 3.5 bar.

The frequency of the sound wave used to vibrate the membrane is selected between 200 Hz and 5 000 Hz. It is expected that additional pressure will be caused by the sound wave and that at higher frequencies this pressure differences will contribute to the bubbles overcoming the surface tension of the

membranes sooner.

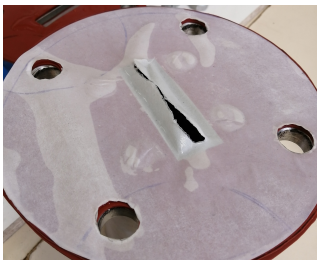

Figure 5.1: The TRISEP® UB70 membrane fractured at a pressure of just over 4 *bar*

The combinations of values for experimental independent variables, for this experiment, were selected using Box-Behnken design. These selected combinations were then used and the dissolved oxygen in the water was measured as an output. A plot of the selected values can be seen in Figure 5.2. It can be seen that the determined values form a box with a centroid. The variable value combinations form the sides of the box.

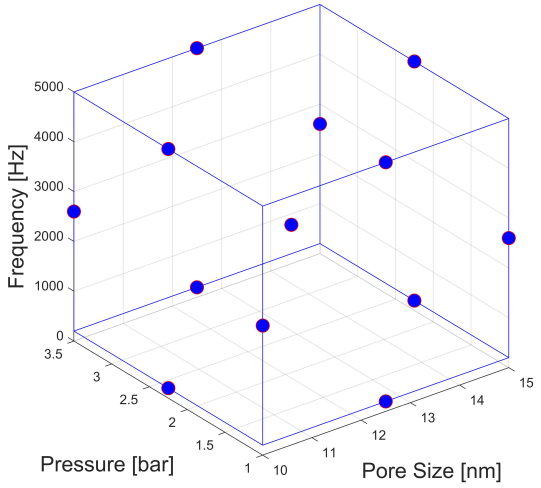

Figure 5.2: 3D Plot representing the variable value combinations for the set of experiments, as determined using Box-Behnken design

5.1.2 Experimental measurements and observations

Experiments are conducted using the different sets of values for the variables, as determined using Box-Behnken. The raw measurements are processed to simplify fitting a response surface to the data. For this set of experiments the dissolved oxygen, the mean bubble size and the zeta potential are measured, as seen in Table 5.2.

Dissolved oxygen (DO_2) is measured using a dissolved oxygen probe. To ensure accuracy multiple measurements are taken of each run. Measurements are taken over time, to determine stability, and the maximum measured dissolved oxygen value is used. It was observed that the DO_2 reaches a plateau before 10 minutes have passed. Therefore all the measurements, recorded in Table 5.2, are taken at 10 minutes running time.

The measurements are recorded in terms of percentage dissolved oxygen and temperature. This is then converted to millilitre dissolved oxygen per litre water. A zero reading of the water used, without additional oxygen added, is taken and subtracted from each reading to determine the increase in dissolved oxygen levels. Table 5.2 gives the increase in dissolved oxygen for each experimental run.

Samples are taken at a sampling tap just before the dissolved oxygen probe and the bubble size and zeta potential are measured using an Anton Paar Litesizer^{TM} . The Litesizer^{TM} uses dynamic light scattering (DLS), electrophoretic light scattering (ELS) and static light scattering (SLS) to determine particle size and zeta potential (Anton-Paar, 2019). These measured values are also given in Table 5.2.

From Table 5.2 it is observed that the average measured DO_2 for two of the sets of variables were 0 mL/L. Both of these measurements were obtained using the SelRO® MPS-34 membrane. One of the properties of nano-bubbles is that they can remain suspended in a mixture for a significant period of time due to their negative surface charge(Meegoda *et al.*, 2018). These two measurements of 0 mL/L could be due to nano-bubbles forming within the water, but not dissolving significantly before reaching the dissolved oxygen probe.

Table 5.2: Experimental data at a water flowrate of 5 L/min

DO_2	Bubble size	Zeta potential	Pore size	Pressure	Frequency
2.8 mL/L	359.2 nm	-12.1 mV	10.0 nm	2.25 bar	200 Hz
0.2 mL/L	293.9 nm	-10 mV	12.5 nm	1.00 bar	200 Hz
1.3 mL/L	358.4 nm	-17 mV	12.5 nm	3.50 bar	200 Hz
0.0 mL/L	386.3 nm	-17.4 mV	15.0 nm	2.25 bar	200 Hz
0.9 mL/L	338.1 nm	-12.6 mV	10.0 nm	3.50 bar	2 600 Hz
0.7 mL/L	386.4 nm	-12.4 mV	10.0 nm	1.00 bar	2 600 Hz
0.9 mL/L	344.5 nm	-21.6 mV	12.5 nm	2.25 bar	2 600 Hz
0.7 mL/L	346.3 nm	-14.6 mV	10.0 nm	2.25 bar	5 000 Hz
1.6 mL/L	240.5 nm	-15.6 mV	12.5 nm	3.50 bar	5 000 Hz
0.1 mL/L	345 nm	-20.4 mV	15.0 nm	3.50 bar	2 600 Hz
0.2 mL/L	372.8 nm	-13.3 mV	12.5 nm	1.00 bar	5 000 Hz
1.1 mL/L	274.6 nm	-8.7 mV	15.0 nm	2.25 bar	5 000 Hz
0.0 mL/L	397.5 nm	-9.3 mV	15.0 nm	1.00 bar	2 600 Hz

5.1.3 Response surface methodology

A function is fit to the data using RStudio (2019) software. Two different approaches are used. The first approach has the nominal pore size of the membrane, oxygen inlet pressure and the frequency of the sound wave used to vibrate the system as the independent variables and dissolved oxygen as the dependent variable. The second approach also uses the bubble size and zeta potential as independent variables along with pore size, pressure and frequency.

Equation 5.1 is used and the values of the coefficients are determined to get an function that describes the data as closely as possible, without "over-fitting" the function to the data. The function investigates the linear and quadratic behaviour of the data.

$$Y = \beta_1(X_1)^2 + \beta_2(X_2)^2 + \beta_3(X_3)^2 + \beta_4 X_1 + \beta_5 X_2 + \beta_6 X_3 + \beta_7 \quad (5.1)$$

The resulting fit has the following coefficients:

$$\begin{aligned}
\beta_1 &= -1.20e^{-2} \\
\beta_2 &= -2.56e^{-1} \\
\beta_3 &= 5.64e^{-8} \\
\beta_4 &= 1.05e^{-1} \\
\beta_5 &= 1.43e^{0} \\
\beta_6 &= -3.30e^{-4} \\
\beta_7 &= 1.27e^{-2}
\end{aligned} \tag{5.2}$$

The resulting Residual standard error is 0.764, the multiple R^2 is 0.534 and the mean square residual is 0.584. The residual standard error of 0.764 mL/L is quite high considering that the mean dissolved oxygen value is 0.808 mL/L. This means the percentage error is 94.6%. The multiple R^2 value indicates that 53.4% of the response can be explained by the predicted value. The mean square residual is an indication of how close the data is to the surface.

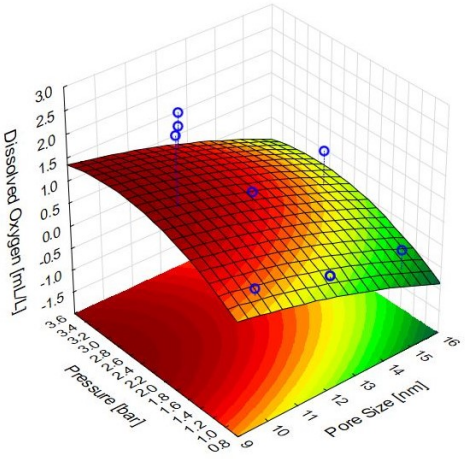

Figure 5.3: Surface plot of dissolved oxygen over pressure and pore size, with blue markers indicating measured data

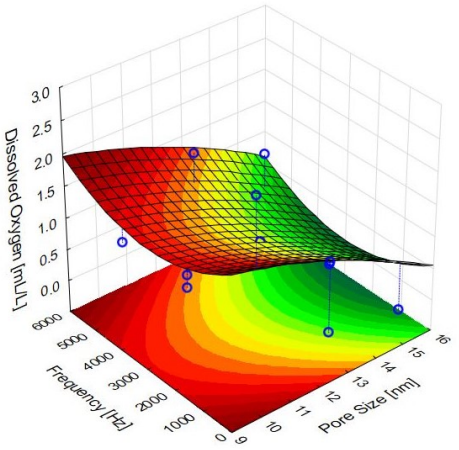

Figure 5.4: Surface plot of dissolved oxygen over frequency and pore size, with blue markers indicating measured data

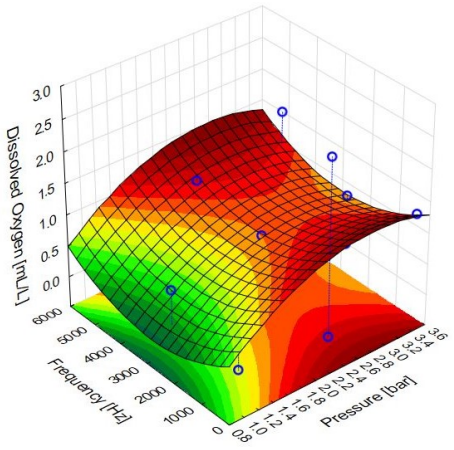

Figure 5.5: Surface plot of dissolved oxygen over frequency and pressure, with blue markers indicating measured data

In Equation 5.1 and 5.2 the form and the coefficients of a surface that was fit to the data is given. In Figures 5.3, 5.4 and 5.5 the plots of the surface are given as dissolved oxygen over two of the three independent variables, with the third variable kept constant at its average value. Each plot includes blue markers, indicating the actual measured data.

It is seen that the measured data are relatively close to the surface, with some exceptions, and the surfaces tend to follow the decline and incline of the data. This correlates with the R^2 value, the standard error and the mean square residual that were determined. Therefore it is accepted that the function is a reasonable representation of the data.

In Figure 5.3, dissolved oxygen over pressure and nominal pore size is plotted at a constant average frequency. The surface is slightly curved, but almost forms a flat surface. From visual inspection, it is determined that the maximum dissolved oxygen is expected at about 2.8 *bar* and at the smallest pore size, within the tested range, of 10 *nm*. Any values of the surface, outside of the tested ranges, as mentioned in Table 5.2, are disregarded.

In Figure 5.4, dissolved oxygen over frequency and pore size is plotted at a constant average pressure. It is observed that two of the visible data markers, most left on the current view of the plot, are far from the surface. Points that are a distance from the surface are expected, as the surface is not a perfect fit to the data. These low DO_2 values are measured at a oxygen inlet pressure

of 1 *bar* and it could be that the membrane lets minimal to zero oxygen pass through at low pressures. Along the frequency axis it is seen that the surface curves and reaches a trough at about 3 000 Hz with maximum values for DO_2 at low and high frequencies. Once again, expected maximums are only considered within the ranges as set out in Table 5.2. From visual inspection the maximum DO_2 is expected at a low frequency of 200 Hz and small pore size of 10 nm.

In Figure 5.3, dissolved oxygen over frequency and pore size is plotted and the expected maximum dissolved oxygen, as determined by visual inspection, is at about 2.8 *bar* and low frequency of 200 Hz.

The determined function is used and different plots are made, varying one of the three independent variables and observing the change that occurs. This is done to visually appreciate the effect of the different independent variables.

In Figures 5.6, 5.7 and 5.8 dissolved oxygen (DO_2) in mL/L is plotted over pressure, in *bar*, and the nominal pore size of the membrane in nm. The frequency of the sound wave that vibrates the setup is varied and the effect is observed. The frequencies are set at 200 Hz, 2 600 Hz and 5 000 Hz as these are the values at which the experiments were conducted.

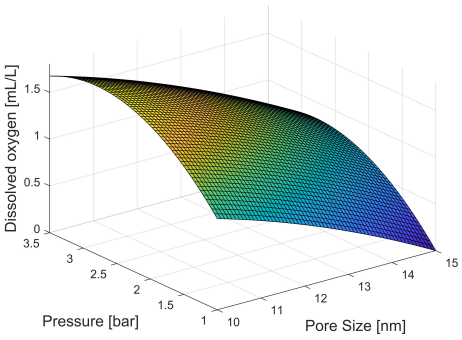

Figure 5.6: Surface plot of dissolved oxygen over pressure and pore size at 200 Hz

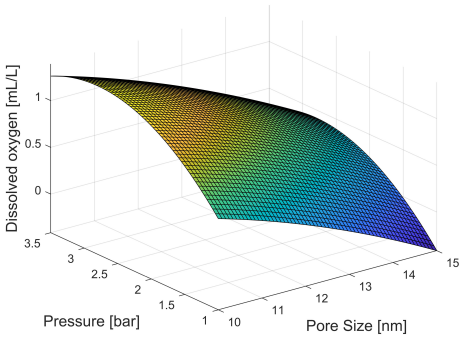

Figure 5.7: Surface plot of dissolved oxygen over pressure and pore size at 2 600 Hz

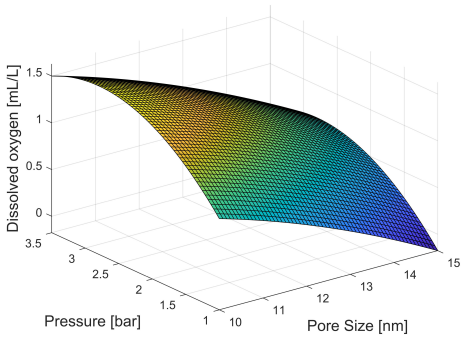

Figure 5.8: Surface plot of dissolved oxygen over pressure and pore size at 5 000 Hz

It can be seen that maximum DO_2 at 200 Hz is higher than the maximum DO_2 at 2 600 Hz. When increasing the frequency to 5 000 Hz the DO_2 increases again to about 1.5 mL/L. From this it is concluded that vibrating the membrane at various frequencies using sound does have an effect on the total amount of dissolved oxygen in the water.

It was expected that acoustic interference will have an effect on the oxygenation as the vibrations could affect how the bubbles form, at what point the bubble will break loose and add extra energy to "push" the oxygen through te membrane.

As discussed in Section 4.1, the flat sheet membranes consists of small cracks, instead of elliptical pores. An explanation for the observed maximum oxygenation at lower frequencies, could be that as the frequency is lower, the cracks in the membrane are "stretched" open for longer time periods, leading to more oxygen permeating the membrane into the water.

In Figures 5.9, 5.10 and 5.11 dissolved oxygen (DO_2) in mL/L is plotted over frequency, in Hz, and the nominal pore size of the membrane in nm. The inlet pressure of the oxygen is varied and the effect is observed. As the pressure is increased from 1 bar to 2.25 bar the surface shifts up and the maximum DO_2 increases. As the pressure is increased from 2.25 bar to 3.5 bar the surface shifts down and the maximum DO_2 decreases.

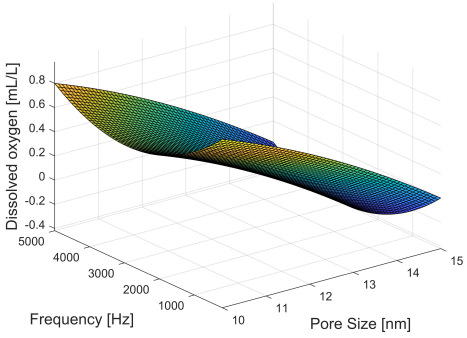

Figure 5.9: Surface plot of dissolved oxygen over frequency and pore size at 1 bar

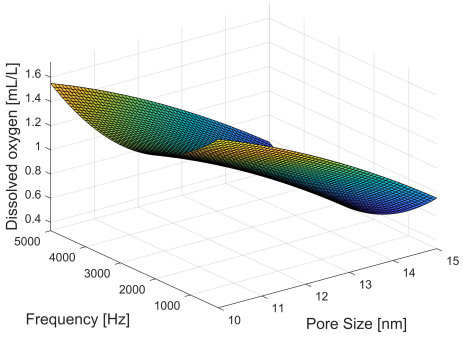

Figure 5.10: Surface plot of dissolved oxygen over frequency and pore size at 2.25 bar

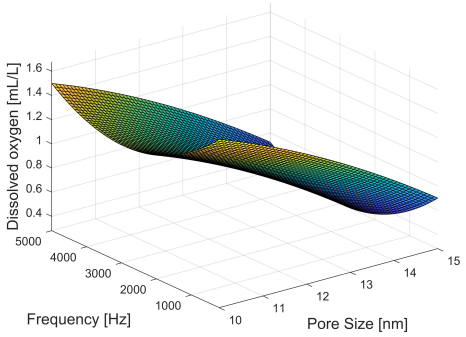

Figure 5.11: Surface plot of dissolved oxygen over frequency and pore size at 3.5 bar

As discussed, upon visual inspection it is observed that the dissolved oxygen increases as the pore size decreases. As discussed in Section 2.6 and seen in Figure 2.13, the bubble size is affected by the nominal pore size of the membrane. As the nominal pore size of the membrane decreases, so the diameter of the bubbles that are formed decreases (Ahmed *et al.*, 2018). As discussed in Section 2.5, as the diameter of the nano-bubbles are reduced, the contact surface area increases and leads to better oxygen transfer.

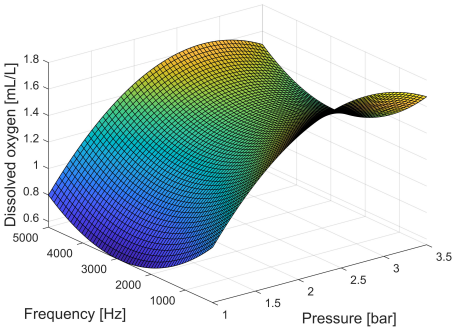

Figure 5.12: Surface plot of dissolved oxygen over frequency and pressure at 10 nm

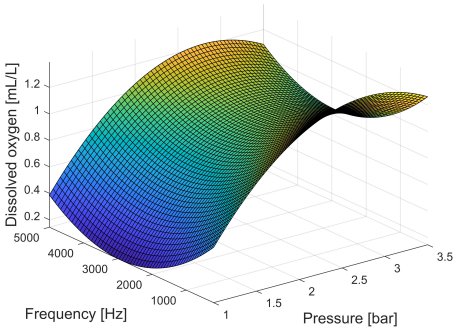

Figure 5.13: Surface plot of dissolved oxygen over frequency and pressure at 12.5 nm

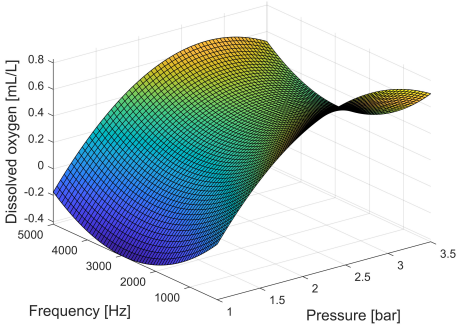

Figure 5.14: Surface plot of dissolved oxygen over frequency and pressure at 15 nm

In Figures 5.12, 5.13 and 5.14 dissolved oxygen (DO_2) in mL/L is plotted over frequency, in Hz, and pressure in bar. The nominal pore size of the membrane is varied and the effect thereof is observed. It can be seen that as the pore size is decreased the surface shifts downward and the maximum DO_2 decreases.

It can be seen, as previously mentioned, that as the pressure increases the maximum DO_2 is expected at about 2.8 bar after which it decreases as the pressure is further increased. This is counter-intuitive as it is expected that as the pressure increases, more oxygen permeates the membrane leading to a higher level of dissolved oxygen. A possible explanation for the drop in DO_2 at higher pressure is that as the pressure is increased, the size of the bubbles decrease because the bubbles break loose from the membrane sooner. As discussed in Section 2.5, one of the characteristics of nano-bubbles are that they can remain suspended in a fluid due to their small size and negative surface

charge (zeta-potential). The higher pressure could lead to smaller bubbles, that instead of immediately dissolving, stay suspended in the water causing a lower DO_2 reading.

In Figure 5.15 a Pareto chart of standardized effects, as generated using Statistica (TIBC), is given. As the name suggests, the chart is a normalised indication of the effect of each variable. The linear and quadratic effects are represented on the chart, with $x1$, $x2$ and $x3$ representing pore size, pressure and frequency, respectively.

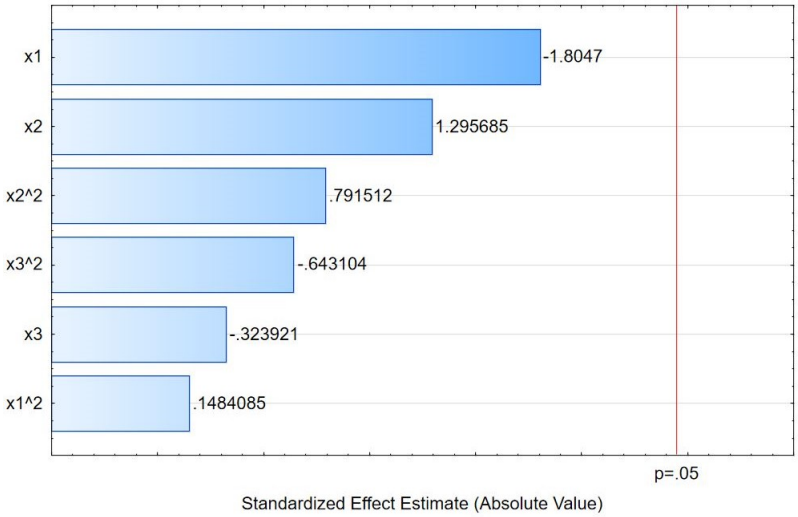

Figure 5.15: Pareto chart of standardized effects

It is seen that the linear effect of the nominal membrane pore size is the greatest, followed by the linear and quadratic effect of the oxygen inlet pressure. The quadratic effect of the frequency used to vibrate the membrane is more than the linear effect thereof. It was expected that the pore size and pressure has the greatest effect on the level of dissolved oxygen.

A second approach is used where the bubble size and zeta potential, as measured using the Anton Paar Litesizer^{TM} , is also used in determining a function that represents the dissolved oxygen along with the pore size, oxygen inlet pressure and the frequency of the sound wave used for vibration.

In Equation 5.3, pore size, pressure, frequency, bubble size and zeta potential, are represented by X_1, X_2, X_3, X_4 and X_5, respectively. it can be seen that the linear and quadratic effects of these variables are included in the equation. The effect of bubble size on zeta potential is also allowed for by the term $\beta_{11}X_4X_5$.

$$\begin{aligned} Y &= \beta_1(X_1)^2 + \beta_2(X_2)^2 + \beta_3(X_3)^2 + \beta_4(X_4)^2 + \beta_5(X_5)^2 \\ &+ \beta_6X_1 + \beta_7X_2 + \beta_8X_3 + \beta_9X_4 + \beta_{10}X_5 + \beta_{11}X_4X_5 + \beta_{12} \end{aligned} \tag{5.3}$$

The resulting fit has the following coefficients:

$$\begin{aligned} \beta_1 &= 8.09e^{-2} \\ \beta_2 &= 4.86e^{-1} \\ \beta_3 &= 4.28e^{-7} \\ \beta_4 &= 3.58e^{-4} \\ \beta_5 &= 9.92e^{-2} \\ \beta_6 &= -2.75e^{0} \\ \beta_7 &= -1.34e^{0} \\ \beta_8 &= -2.23e^{-3} \\ \beta_9 &= -2.22e^{-1} \\ \beta_{10} &= 3.02e^{0} \\ \beta_{11} &= -2.41e^{-4} \\ \beta_{12} &= 7.72e^{1} \end{aligned} \tag{5.4}$$

The resulting Residual standard error is 0.87 and the multiple R^2 is 0.90. The residual standard error of 0.87 mL/L is quite high considering that the mean dissolved oxygen value is 0.81 mL/L. This means the percentage error is 107.2%. The multiple R^2 value indicates that 90.0% of the response can be explained by the predicted value.

When comparing the two different approaches, as described in Equation 5.1 and 5.3 it is seen that the second approach, Equation 5.3, has a higher R^2 value, indicating that it is a better representation of the data than the first approach. The bubble size and zeta potential are not independent variables that can be controlled, but rather dependant variables.

To determine the effect of bubble size and zeta potential on dissolved oxygen a function was fit to the data representing dissolved oxygen (Y) over bubble size (X_4) and zeta potential (X_4) resulting in an equation of form,

$$Y = \beta_1(X_4)^2 + \beta_2(X_5)^2 + \beta_3 X_4 + \beta_4 X_5 + \beta_5 X_4 X_5 + \beta_6 \tag{5.5}$$

With the following coefficients:

$$\begin{aligned} \beta_1 &= -1.07e^{-04} \\ \beta_2 &= -1.26e^{-02} \\ \beta_3 &= 8.09e^{-02} \\ \beta_4 &= -8.31e^{-01} \\ \beta_5 &= 1.39e^{-03} \\ \beta_6 &= -1.65e^{+01} \end{aligned} \tag{5.6}$$

A plot of the surface, represented by Equation 5.5 with coefficients as in Equation 5.7, is seen in Figure 5.16. The blue markers represent the measured data, as seen in Table 5.2. Figures 5.17 and 5.18 are plots of the same surface, viewed as DO_2 over bubble size and over zeta potential, respectively.

In Figures 5.16 and 5.16 it is seen that at a zeta potential between $-9\ mV$ and $-22\ mV$, the dissolved oxygen decreases as the bubble size increases. As discussed in Section 2.5, as the average bubble diameter decreases the contact surface area increases, leading to improved oxygen transfer and higher dissolved oxygen levels.

It can be seen that at smaller bubble sizes, more negative zeta potentials lead to higher levels of dissolved oxygen and at larger bubble sizes it is expected that the opposite is true. It is expected that more negative zeta potential

is associated with smaller bubble size and, as discussed, smaller bubbles are expected to lead to better dissolved oxygen levels.

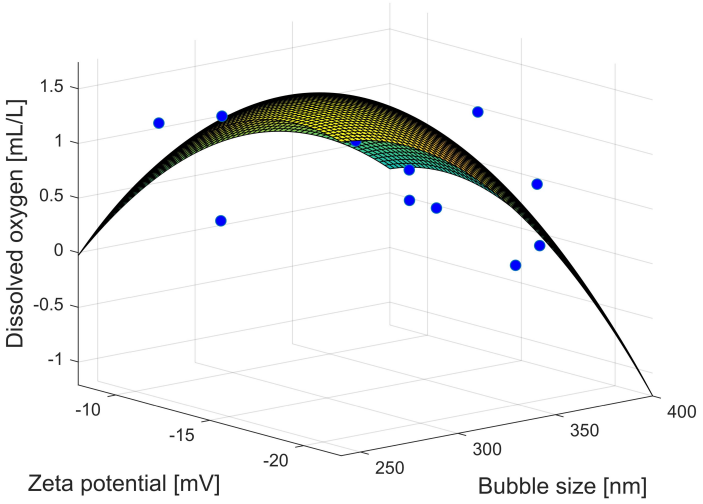

Figure 5.16: Surface plot of dissolved oxygen over bubble size and zeta potential

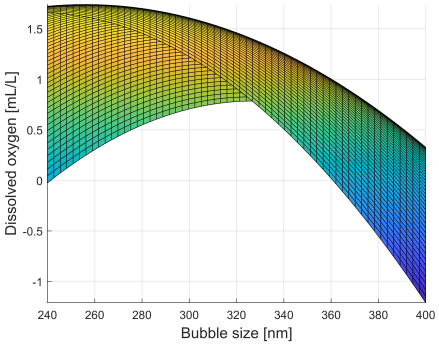

Figure 5.17: Surface plot of dissolved oxygen over bubble size and zeta potential with blue markers indicating measured data

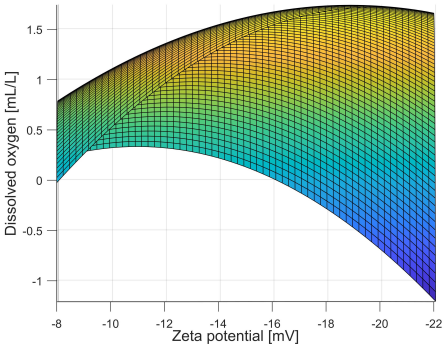

Figure 5.18: Surface plot of dissolved oxygen over bubble size and zeta potential

5.1.4 Optimisation of response surface

A Genetic Algorithm (GA) is used to determine a near optimum solution for the function determined in Section 5.1.3, Equation 5.1. A near optimum point

is determined, within the range that the variables were tested in.

It is desired to determine a near optimum point, as the overarching aim is to sufficiently oxygenate a human intravenously. Determining the near optimum would give insight into the possible design of future intravenous oxygenation devices.

As the population size and number of generations greatly affect the outcome of a GA, different combinations of large and small values for population size and number of generations are used, as seen in Table 5.3.

Table 5.3: Comparison of results obtained using a Genetic Algorithm with different population sizes and number of generations

Population size	**Number of generations**	**Number of generations reached**	**Best individual measured**	**Pore size** **Pressure** **Frequency**
50	300	112	1.798	10 nm 2.797 bar 210.751 Hz
200	300	109	1.802	10 nm 2.797 bar 200 Hz
50	600	62	1.802	10 nm 2.797 bar 200 Hz
200	600	90	1.805	10 nm 2.797 bar 200 Hz

It can be seen in Table 5.3 that all the runs except the first one has exactly the same value best individual and the values, when using a population size of 50 and 300 generations, is very close to the other runs. When comparing the results of the GA to the plots in Figures 5.6 to 5.14 both indicate the same

expected near optimum at a nominal membrane pore size of 10 nm, a pressure of 2.797 bar and a sound frequency of 200 Hz.

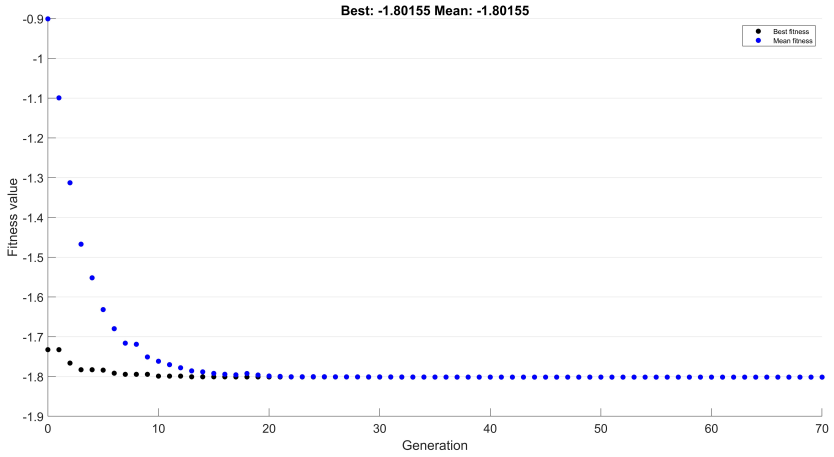

Figure 5.19: Plot of the best individual and the mean of each generation

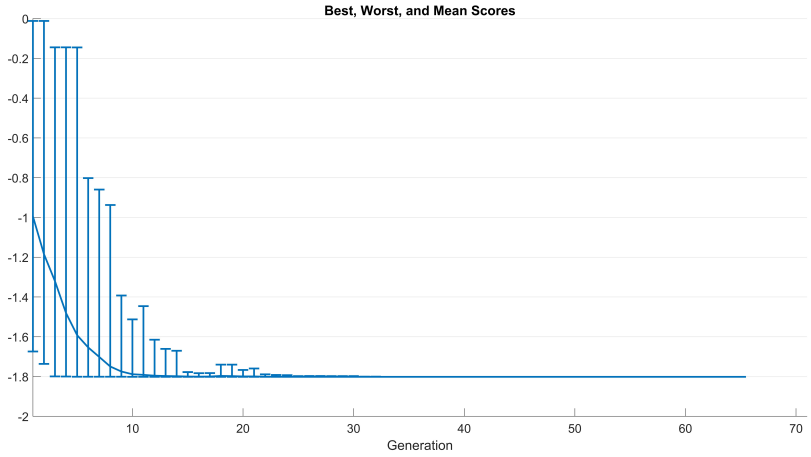

Figure 5.20: Plot of the best, worst and mean scores for each generation

Note that the GA used can only minimise, therefore the fuction was multiplied by -1. The values of the y-axis of the plots, as seen in Figures 5.19 and 5.20, should be multiplied by -1 to determine the actual value. It is seen in Figure 5.19 that the best and the mean fitness decline until about the 20th generation is reached, where it plateaus. It can also be seen that the best and the mean fitness converge to one value. The same is seen in Figure 5.20, that for each

following generation the range between best and worst individual decreases as the values converge to the best individual.

5.1.5 Conclusion: Generating bubbles using flat sheet membranes

The experiments were designed using Box-Behnken design and conducted with sufficient repetitions to improve accuracy of collected data. The data was analysed and surfaces were fit to the data.

Plots were made and upon visual inspection it was observed that increased dissolved oxygen levels are expected at smaller pores sizes. As expected, an increase in pressure leads to en increase in dissolved oxygen, but only up to 2.8 bar, after which there is a drop in dissolved oxygen. This drop was attributed to the stability of nano-bubbles. It was observed that the dissolved oxygen decreases as the frequency, at which the system is vibrated, increases until the frequency reaches a trough at about 3 000 Hz. From 3 000 Hz onward the dissolved oxygen increases as the frequency increases. A proposed explanation for this is that the cracks in the membrane, as discussed in Section 4.1, are stretched open by the vibrations, and at low frequency the time which it is stretched open for is longer at low frequencies, causing more oxygen to pass through the membrane, leading to higher levels of dissolved oxygen.

A Pareto chart of standardized effects was generated and the linear and quadratic effects of the different variables were compared. The linear effects of pore size and pressure have the largest significance, but it was determined that the frequency at which the system is vibrated does have an effect on the level of dissolved oxygen in the water.

The effect of bubble size and zeta potential on the level of dissolved oxygen in water was investigated. It was expected that a decrease in bubble diameter would lead to a increase in dissolved oxygen levels. At a zeta potential between $-9\ mV$ and $-22\ mV$ it was observed, as expected, that a decrease in bubble diameter leads to an increase in dissolved oxygen. It is expected that as the bubble size decreases the zeta potential becomes more negative. As a more negative zeta potential is associated with smaller bubble sizes and smaller bubbles are associated with higher levels of dissolved oxygen it was expected that as zeta-potential becomes more negative, the dissolved oxygen would increase.

A genetic algorithm was used to determine the near optimum combination of

variables that is expected to give the best dissolved oxygen levels. The results coincided with the results obtained from visual inspection and the expected optimum point was determined to be at a pore size of 10 nm, a pressure of 2.8 bar and a frequency of 200 Hz.

5.2 Generating bubbles using tubular ceramic membranes

A second iteration is done using tubular ceramic membranes. Membranes are selected using Box-Behnken design, but also taking into consideration standard pore sizes available and local supplier stock. The experiment is conducted and the data is analysed to determine a response surface which is a good representation of the data. The surface is analysed using analysis of variance (ANOVA) to determine if it is a good representation of the actual measured data. The surface is then optimised to determine where the expected optimum is.

5.2.1 Box-Behnken design for experimental variable selection

Box-Behnken is an efficient method by which the different combinations of variables are selected. The Box-Behnken design method requires fewer runs than a normal factorial technique, but still has enough data points to fit a representative surface in the selected area. The ranges for the variables can be seen in Table 5.4 below.

Table 5.4: The ranges of the variables as used in Box-Behnken

Variable	Minimum Value	Maximum Value
Pore Size	50 nm	200 nm
Pressure	1 bar	4 bar
Frequency	200 Hz	5 000 Hz

Experiments done by Ahmed *et al.* (2018) are done using membranes with a 100 nm and 1 000 nm pore size and it was concluded that a smaller membrane pore size leads to smaller mean bubble size. As Ahmed *et al.* (2018) reports that nano-bubbles are generated using these membranes and as nano-bubbles are detected in the experiments done using flat sheet membranes, the pore

size range is selected between 50 nm and 200 nm. This range covers the gap between work done in Section 5.1 and the work done by Ahmed *et al.* (2018), but still overlapping with the work done by Ahmed *et al.* (2018) to be able to validate results and compare performance.

The pressure range is chosen between 1 bar and 4 bar as in initial correspondence the membrane suppliers suggested that a maximum pressure of 4 bar be used to ensure the membrane does not break.

The frequency of the sound wave used to fibrate the membrane was selected between 200 Hz and 5 000 Hz. It is expected that the sound will assist the oxygen pressure as driving force to "press" oxygen through the membrane. It is expected that lower frequencies will give longer additional drive than higher frequencies that will cause short bursts of additional "pressure", therefore the lower frequency range was selected.

The combinations of values for experimental variables, for this experiment, are selected using Box-Behnken design. A plot of the selected values can be seen in Figure 5.21. It can be seen that the determined values form a box with a centroid. The variable value combinations form the sides of the box.

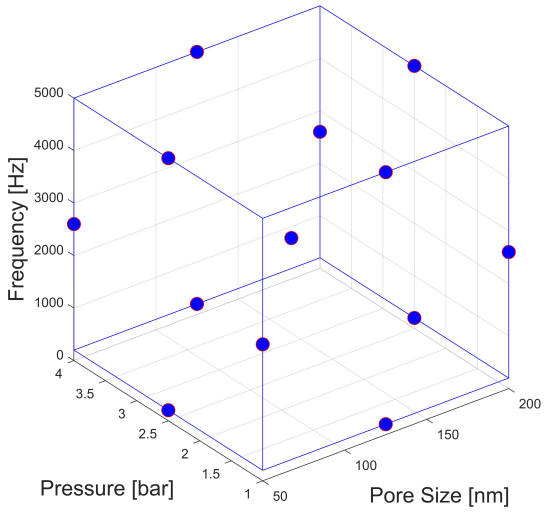

Figure 5.21: 3D Plot representing the variable value combinations for the set of experiments, as determined using Box-Behnken design

5.2.2 Experimental measurements and observations

Experiments are conducted using the different sets of values for the variables, as determined using Box-Behnken. The raw measurements are processed to simplify fitting a response surface to the data.

Dissolved oxygen is measured using a dissolved oxygen probe. The measurements are recorded in terms of percentage dissolved oxygen and temperature. This is then converted to millilitre oxygen per litre water. A zero reading of the water used, without additional oxygen added, is taken and subtracted from each reading to determine the increase in dissolved oxygen levels. Table 5.5 gives the increase in dissolved oxygen for each experimental run.

5.2.3 Experimental measurements and observations

Table 5.5: Experimental data at a water flowrate of 3 L/min

DO_2	Standard deviation	Pore size	Pressure	Frequency
0 mL/L	0.007	50 nm	2.5 bar	200 Hz
0.355 mL/L	0.078	100 nm	1 bar	200 Hz
0.03 mL/L	0.001	100 nm	4 bar	200 Hz
0.16 mL/L	0.007	200 nm	2.5 bar	200 Hz
0.305 mL/L	0.077	50 nm	4 bar	2 600 Hz
0.14 mL/L	0.007	50 nm	1 bar	2 600 Hz
0.47 mL/L	0.276	100 nm	2.5 bar	2 600 Hz
0.08 mL/L	0.001	50 nm	2.5 bar	5 000 Hz
0.78 mL/L	0.049	100 nm	4 bar	5 000 Hz
0.26 mL/L	0.014	200 nm	4 bar	2 600 Hz
1.08 mL/L	1.07	100 nm	1 bar	5 000 Hz
0 mL/L	0.055	200 nm	2.5 bar	5 000 Hz
0 mL/L	0.119	200 nm	1 bar	2 600 Hz

5.2.4 Response surface methodology

A key part of Response Surface Methodology (RSM) is to determine a surface that is a good representation of the actual measured data obtained during the experimentation phase. The data is processed and RStudio is used to fit a function to the data. The function is analysed using ANOVA to determine if it is a good representation of the actual measured data.
The data in Table 5.5 is imported into Rstudio and fitted to a surface with the following form

$$Y = \beta_1(X_1)^2 + \beta_2(X_2)^2 + \beta_3(X_3)^2 + \beta_4 X_1 + \beta_5 X_2 + \beta_6 X_3 + \beta_7 \quad (5.7)$$

The resulting fit has the following coefficients:

$$\begin{aligned} \beta_1 &= -7.86e^{-5} \\ \beta_2 &= 4.61e^{-2} \\ \beta_3 &= -2.17e^{-9} \\ \beta_4 &= 1.95e^{-2} \\ \beta_5 &= -2.47e^{-1} \\ \beta_6 &= 8.39e^{-5} \\ \beta_7 &= -5.66e^{-1} \end{aligned}$$

The resulting Residual standard error is 0.28, the multiple R^2 is 0.64 and the mean square residual is 0.078. The residual standard error of 0.28 mL/L gives a percentage error of close to 100%. The multiple R^2 value indicates that 64.3% of the response can be explained by the predicted value.

The mean square residual is an indication of how close the data is to the surface. The mean square residual of this data set is lower than that of the previous data set, seen in Table 5.2. From this it is concluded that the measured data points are closer to the generated surface for this set of experiments than for the previous set.

When comparing the multiple R^2 value of this set to the previous one, it is seen that for this set the multiple R^2 value is higher, therefore a higher percentage of the response can be explained by the predicted value, than in the previous set.

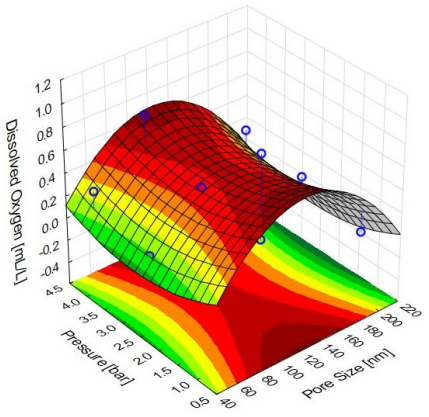

Figure 5.22: Surface plot of dissolved oxygen over pressure and pore size, with blue markers indicating measured data

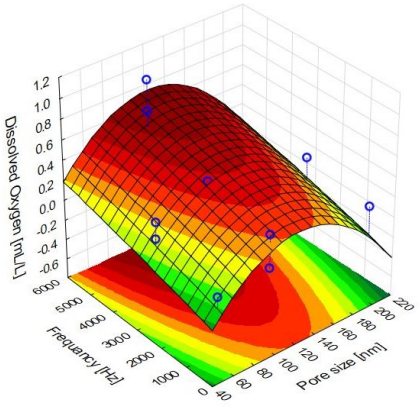

Figure 5.23: Surface plot of dissolved oxygen over frequency and pore size, with blue markers indicating measured data

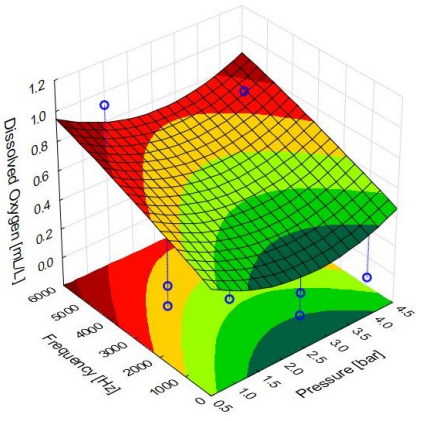

Figure 5.24: Surface plot of dissolved oxygen over frequency and pressure, with blue markers indicating measured data

In Equation 5.7 and 5.8 the form and the coefficients of a surface that was fit to the data is given. In Figures 5.22, 5.23 and 5.24 the plots of the surface are given as dissolved oxygen over two of the three independent variables, with the third variable kept constant at it's average value. Each plot includes blue markers, indicating the actual measured data. It is observed that the blue markers are relatively close to the surface. This is expected as the mean

square residual has a low value.

In Figures 5.25, 5.26 and 5.27 dissolved oxygen (DO_2) in mL/L is plotted over pressure, in *bar*, and the nominal pore size of the membrane in nm. The frequency of the sound wave that vibrates the setup is varied and the effect is observed. The frequencies are set at 200 Hz, 2 600 Hz and 5 000 Hz as these are the values at which the experiments were conducted.

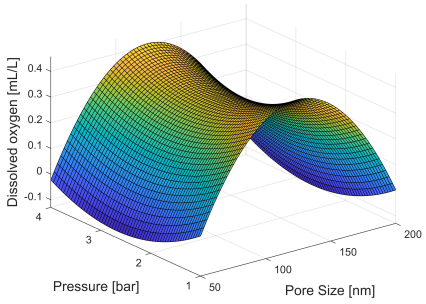

Figure 5.25: Surface plot of dissolved oxygen over pressure and pore size at 200 Hz

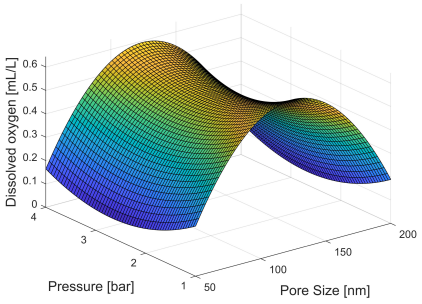

Figure 5.26: Surface plot of dissolved oxygen over pressure and pore size at 2 600 Hz

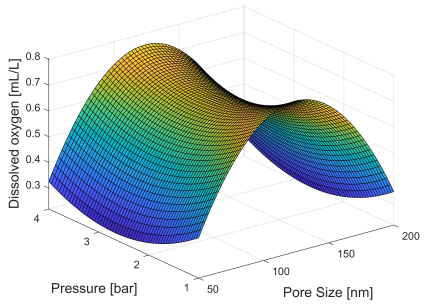

Figure 5.27: Surface plot of dissolved oxygen over pressure and pore size at 5 000 Hz

Upon visual inspection it is observed that the dissolved oxygen reaches a maximum value as the pore size reaches a value of about 125 nm. It is expected that a smaller pore size would lead to higher DO_2 as smaller bubbles are associated with smaller pore size (Ahmed *et al.*, 2018) and smaller bubbles have a larger contact surface area, for the same total volume, than larger bubbles. During experimentation it was observed that the membrane with the 100 nm nominal pore size, formed large bubbles at certain points on the membrane.

These "leaks" could lead to increased levels of DO_2. As the overarching aim is to develop a device for intravascular blood oxygenation, large bubbles forming would be problematic, as it could be fatal (Yuan, 2016).

As the frequency is increased, the surface shifts upward. This increase associated with increased frequency, is almost linear, as seen in Figures 5.28, 5.29 and 5.30. It was expected that lower frequencies would lead to better oxygenation, but the opposite is observed for the tubular ceramic membranes. The almost linear increase in DO_2 could be attributed to the possibility that at higher frequencies, shorter pulses add to the driving force "pressing" oxygen through the membrane, leading to smaller bubbles being formed and as discussed, smaller bubbles are expected to lead to better oxygenation.

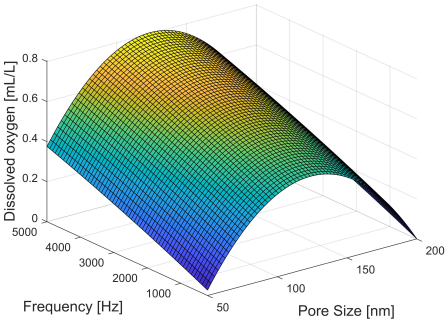

Figure 5.28: Surface plot of dissolved oxygen over frequency and pore size at 1 bar

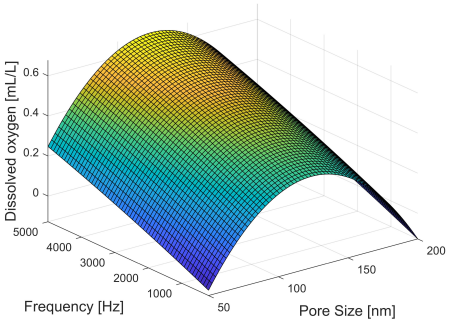

Figure 5.29: Surface plot of dissolved oxygen over frequency and pore size at 2.5 bar

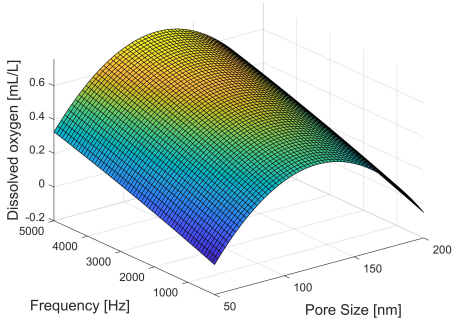

Figure 5.30: Surface plot of dissolved oxygen over frequency and pore size at 4 bar

It can be seen that as the pressure is increased, from 1 *bar* to 2.5 *bar* the maximum dissolved oxygen decreases. As the pressure is further increased from 2.5 *bar* to 4 *bar* the maximum DO_2 is increased. It is expected that as the pressure is increased, the DO_2 increases as well, because pressure is the driving force behind "pressing" the oxygen through the membrane.

A possible explanation for the observed behaviour is that at low pressures oxygen permeates the membrane, forming larger bubbles due to the surface tension between the membrane and oxygen bubble causing the bubble to stay on the surface of the membrane for a longer time period, causing the bubble to continue growing, before it finally becomes big enough and breaks loose from the surface. As the pressure increases the surface tension is overcome sooner, leading to smaller bubbles being formed. These smaller bubbles could then stay suspended in the water, leading to a lower dissolved oxygen level in the water.

The increase in DO_2 as the pressure is increased from 2.5 *bar* to 4 *bar* could be due to decreased bubble size leading to increased DO_2. It could also be attributed to more oxygen permeating the membrane.

In Figures 5.31, 5.32 and 5.33 the plot for DO_2 over frequency and pressure is given at different nominal membrane pore sizes. From visual inspection the maximum level of dissolved oxygen is expected at a pore size close to 125 nm, a low pressure of 1 *bar* or high pressure of 4 *bar* and maximum frequency of 5000 Hz.

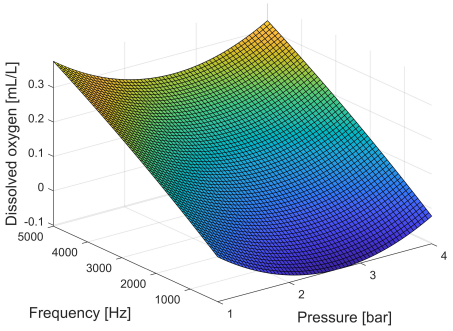

Figure 5.31: Surface plot of dissolved oxygen over frequency and pressure at 50 nm

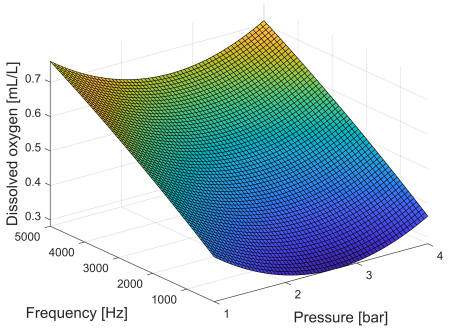

Figure 5.32: Surface plot of dissolved oxygen over frequency and pressure at 100 nm

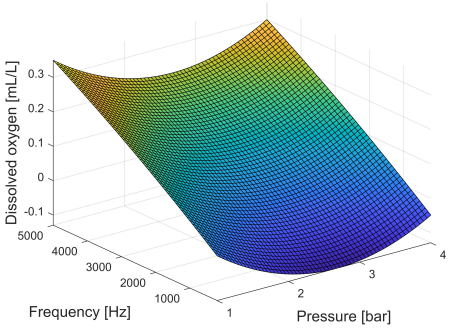

Figure 5.33: Surface plot of dissolved oxygen over frequency and pressure at 200 nm

In Figure 5.34 a Pareto chart of standardized effects is given with $x1$, $x2$ and $x3$ representing pore size, pressure and frequency, respectively. The linear and quadratic effect of each variable is investigated. It is seen that the quadratic component of pore size has the greatest effect on the system. The parameter with the second greatest effect is frequency and thirdly is the quadratic component of pressure.

It is expected that pore size and pressure have the greatest effect on the system, but it is interesting to notice the significance of the effect of frequency. This could be due to the fact that the frequency adds to the driving force "pressing" oxygen through the membrane, but also as the frequency vibrates the membranes a slight shear force could occur breaking the surface tension between the oxygen and the membrane surface.

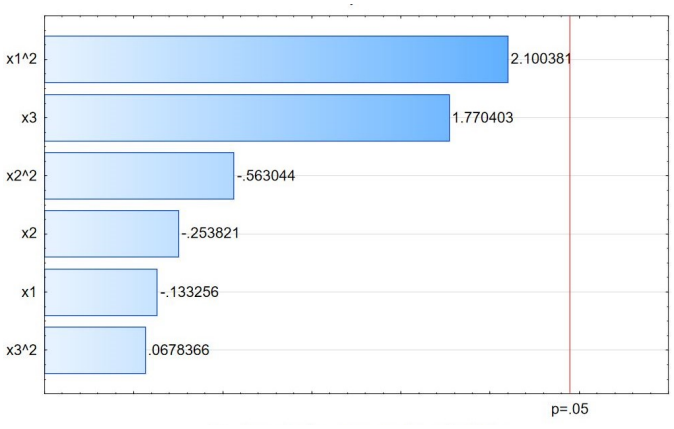

Figure 5.34: Pareto chart of standardized effects

5.2.5 Optimisation of response surface using a genetic algorithm

A Genetic Algorithm (GA) is used to determine a near optimum solution for the function as determined in Section 5.2.4. A near optimum point is determined, within the range that the variables were tested is.

As the population size and number of generations greatly affect the outcome of a GA, different combinations of large and small values for population size and number of generations are used, as seen in Table 5.6.

Table 5.6: Comparison of results obtained using a Genetic Algorithm with different population sizes and number of generations

Population size	**Number of generations**	**Number of generations reached**	**Best individual measured**	**Pore size** **Pressure** **Frequency**
50	300	300	0.751	123.845 nm 3.991 bar 4 950.603 Hz
200	300	137	0.805	123.871 nm 1.000 bar 5 000 Hz
50	600	600	0.802	123.869 nm 1.004 bar 4 958.753 Hz
200	600	135	0.805	123.871 nm 1.000 bar 5 000 Hz

It can be seen in Table 5.6 that all the runs determined a near optimum point at a pore size of 123.8 nm and frequency close to 5 000 Hz. The first run determined a point at close to 4 bar, where the other tree runs determined the near optimum to be at 1 bar. The results correlate with what is expected after

visual inspection of the plots shown in this section.

It is seen in Figure 5.35 that the best and the mean fitness decline until about the 80th generation is reached, where it plateaus. It can also be seen that the best and the mean fitness converge to one value. The same is seen in Figure 5.36, where for each following generation the range between best and worst individual decreases as the values converge to the best individual. Note that the GA used can only minimise, therefore the fuction was multiplied by -1. The values of the y-axis of the plots, as seen in Figures 5.35 and 5.36, should be multiplied by -1 to determine the actual value.

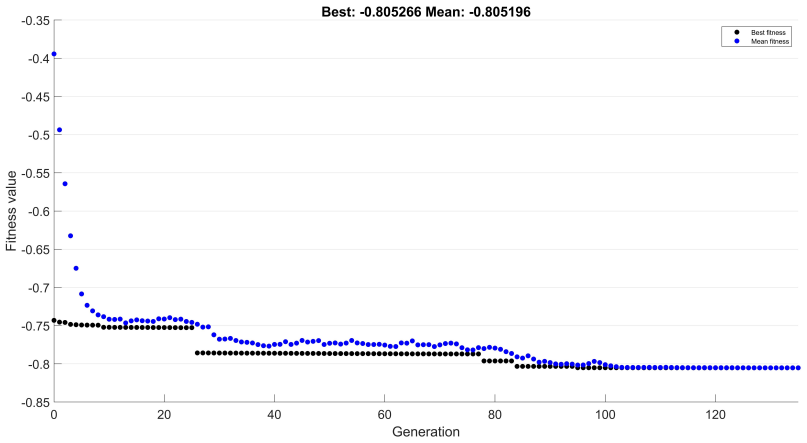

Figure 5.35: Plot of the best individual and the mean of each generation

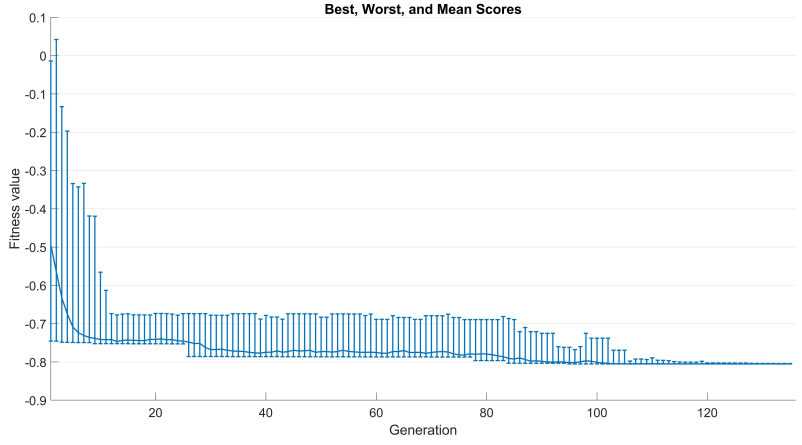

Figure 5.36: Plot of the best, worst and mean scores for each generation

As discussed it was determined that the frequency at which the system is vibrated has a significant effect on the dissolved oxygen level in the water. As the previous set of experiments were only conducted up to a frequency of 5 000 Hz another set of experiments were conducted with a range of higher frequencies, as seen in Table 5.7. Upon further discussion with the suppliers of the membranes it was confirmed that the membranes can withstand higher pressures, therefore the pressure range for this set of experiments was also increased to a maximum pressure of 4.5 bar.

Table 5.7: The ranges of the variables as used in Box-Behnken

Variable	**Minimum Value**	**Maximum Value**
Pore Size	50 nm	200 nm
Pressure	1 bar	4.5 bar
Frequency	4 000 Hz	16 000 Hz

The sets of variables to be used for the experiments was again selected using Box-Behnken design. During experimentation the membrane with the 100 nm pore size developed a major leak, therefor the data obtained using this membrane was disregarded. The remaining data can be seen in Table 5.8.

Table 5.8: Experimental data at a water flowrate of 3 L/min

DO2	**Standard deviation**	**Pore size**	**Pressure**	**Frequency**
1.018	0.012	50	3	4 000
0.968	0.325	200	3	4 000
1.169	0.008	50	5	10 000
0.899	0.014	50	1	10 000
0.935	0.126	50	3	16 000
1.904	0.007	200	5	10 000
1.202	0.051	200	3	16 000
0.228	0.073	200	1	10 000

The data in Table 5.8 is imported into Rstudio and fitted to a surface with the following form

$$Y = \beta_1(X_2)^2 + \beta_2 X_1 + \beta_3 X_2 + \beta_4 X_3 + \beta_5 X_1 X_2 + \beta_6 X_1 X_3 + \beta_7 \quad (5.8)$$

The resulting fit has the following coefficients:

$$\begin{aligned}
\beta_1 &= 5.00e^{-03} \\
\beta_2 &= -8.33e^{-03} \\
\beta_3 &= -7.92e^{-02} \\
\beta_4 &= -1.62e^{-05} \\
\beta_5 &= 2.34e^{-03} \\
\beta_6 &= 1.78e^{-07} \\
\beta_7 &= 1.32e^{+00}
\end{aligned}$$

The function has a R^2 value of 0.998 and a mean square residual of 0.003. The multiple R^2 value indicates that 99.8% of the response can be explained by the predicted value. The mean square residual of 0.003 indicates that the date is very close to the surface. This is expected as the remaining experimental points, after the 100 nm membrane was removed, represent the "sides" of the Box-Behnken design. The fact that the "middle" of the box was removed makes it easier to determine a surface that fits through all the data points.

In Figure 5.37 it can be seen that as the pressure is increased it is expected that the dissolved oxygen increase. It can also be seen that the maximum DO_2 is expected at a high pressure and large pore size. In Figure 5.38 it is seen that the surface is almost flat. It can be seen that there is a slight increase in DO_2 as the frequency increases. In Figure 5.39 it can be seen that the maximum DO_2 is expected at high pressure and high frequency.

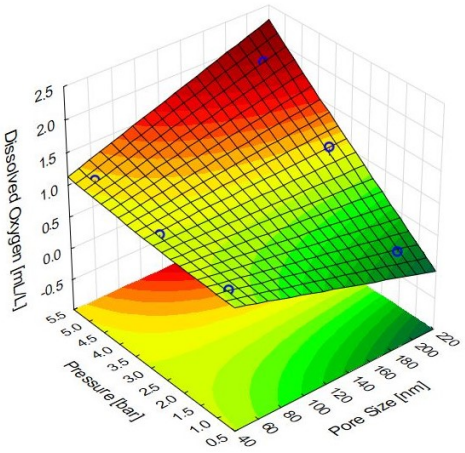

Figure 5.37: Surface plot of dissolved oxygen over pressure and pore size, with blue markers indicating measured data

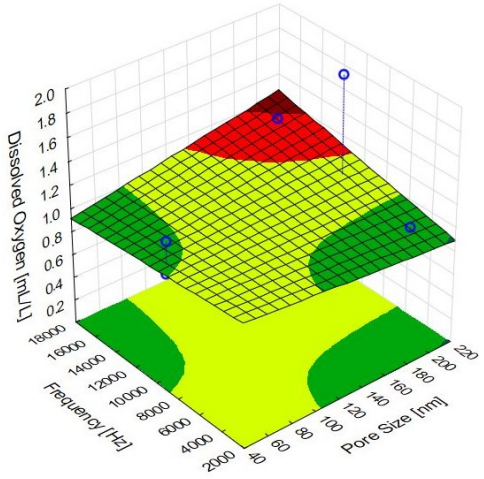

Figure 5.38: Surface plot of dissolved oxygen over frequency and pore size, with blue markers indicating measured data

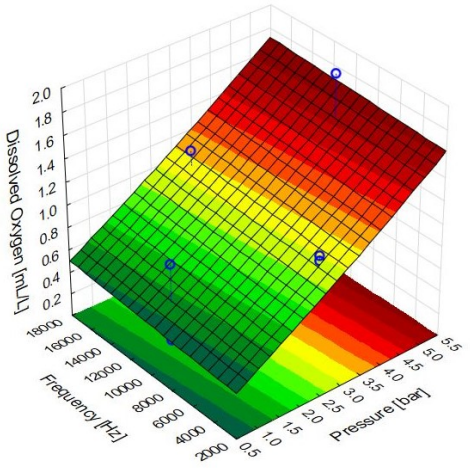

Figure 5.39: Surface plot of dissolved oxygen over frequency and pressure, with blue markers indicating measured data

To summarize, in Figures 5.37, 5.38 and 5.39 it can be seen that the maximum DO_2 is expected at a high pressure, large pore size and high frequency. This is intuitive, as larger pore sizes let's more oxygen through, higher pressure "presses" more oxygen through the membrane into the water and the higher

frequency is expected to reduce bubble size, leading to higher dissolved oxygen levels.

Figure 5.40 gives the Pareto chart of standardized effects, again with $x1$, $x2$ and $x3$ representing pore size, pressure and frequency, respectively. It is seen that the pressure has the most significant effect on the dissolved oxygen, followed by the combined effect of pore size and pressure.

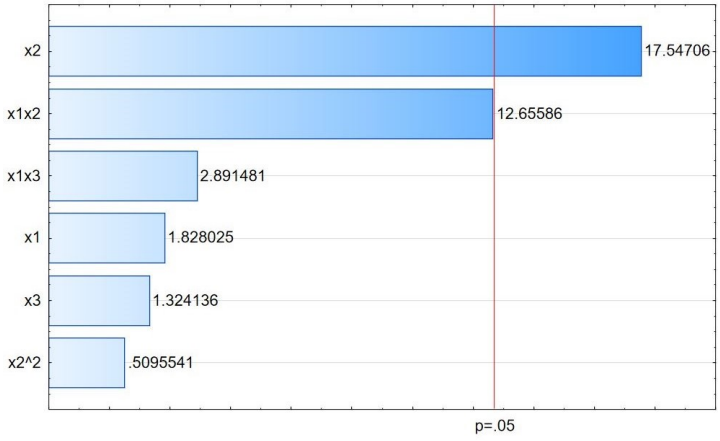

Figure 5.40: Pareto chart of standardized effects

Further data analysis was conducted by combining the two sets of data obtained using the tubular ceramic membranes. All data obtained using the 100 *nm* membrane were excluded, due to the fact that leaks were suspected.

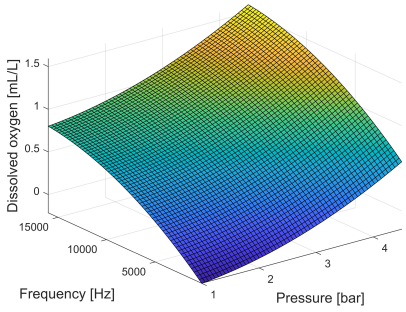

Figure 5.41: Surface plot of dissolved oxygen over frequency and pressure, obtained from combining the two sets of data recorded using tubular ceramic membranes

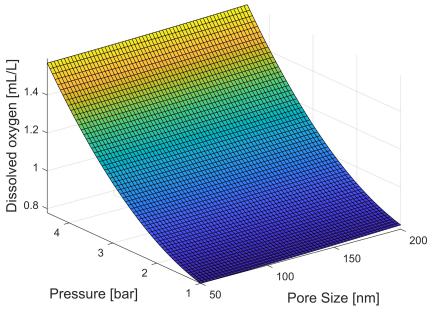

Figure 5.42: Surface plot of dissolved oxygen over pressure and pore size, obtained from combining the two sets of data recorded using tubular ceramic membranes

The resulting function, as represented in Figures 5.41 and 5.42, was analysed using ANOVA and determined to have a multiple R^2 value of 0.647. The multiple R^2 value indicates that 64.7% of the response can be explained by the predicted value. From this it can be concluded that the function is an acceptable representation of the measured data.

In Figures 5.41 and 5.42 it can be seen that the DO_2 increases as frequency, pressure and pore size are increased, respectively. From visual inspection it is determined that the increase in DO_2 associated with pore size is least significant. This behaviour is expected as an increase in pressure increases the amount of oxygen permeating the membrane is increased. The higher pressure could also lead to reduced bubble size, as the surface tension of the membrane is overcome sooner, leading to a larger contact surface area between oxygen and water wich leads to better oxygen transfer. The increase in DO_2 associated with pore size is also expected, as the larger pores has less resistance for the oxygen to permeate the membrane.

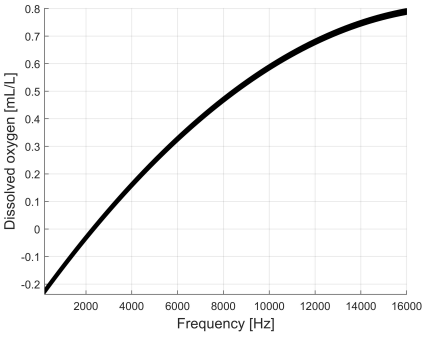

Figure 5.43: Side view of a surface plot of dissolved oxygen over frequency and pore size, obtained from combining the two sets of data recorded using tubular ceramic membranes

Figure 5.43 is a side view of a surface plot of DO_2 over frequency and pore size, highlighting the increase in DO_2 associated with increased frequency. It can be seen that the gradient starts to decline at higher frequency which could indicate a maximum point being reached, but this should be investigated further. Initially it was expected that lower frequencies would lead to higher levels of dissolved oxygen, but it was determined that higher frequencies improve DO_2 levels. Possible reasons for this include that the shorter bursts of energy lead to smaller bubbles being formed, which, as discussed, leads to increased transfer contact area between oxygen and water. Another possible explanation could be that the higher frequency vibration of the membrane causes bubbles

to shear off the membrane, leading the smaller bubble sizes. It could also be that the vibrations agitate the water leading to better oxygen dissolution.

5.2.6 Conclusion: Generating bubbles using tubular ceramic membranes

Experiments were conducted using three different ceramic membranes, as discussed in Section 4.2. Different combinations of variables within a certain range were used, as designed using Box-Behnken design. Two different sets of experiments were conducted and the data analysed. A function was fitted to the data and analysed using ANOVA.

The function determined from the first set of data, was analysed and the expected optimum was determined to be at a pore size of 123 nm, a pressure of 1 bar and a frequency of 5 000 Hz. Parabolic behaviour was observed for DO_2 over pore size and DO_2 over pressure. Along the frequency axis a almost linear increase in DO_2 was observed as the frequency is increased. The expected optimum for the pore size was attributed to possible leaks in the 100 nm membrane, leading to higher levels of DO_2. The expected optimum pressure of 1 bar was attributed to larger bubbles forming due to the low pressure. These larger bubbles are expected to have a less negative zeta potential, causing them to dissolve quicker than smaller bubbles. The increase in DO_2 as the frequency is attributed to higher frequencies attributing to the driving force, "pressing" oxygen through the membrane, in shorter "bursts" than lower frequencies. These shorter bursts could lead to smaller bubbles, increasing the total contact surface area between the oxygen bubbles and the water.

A second set of experiments, using tubular ceramic membranes, were conducted using a increased pressure range and using higher frequencies. For this set of experiments increasingly large leaks were observed when using the 100 nm membrane, therefore the data obtained using this membrane were disregarded. The resulting plots suggested a almost linear increase in DO_2 as pore size, pressure and frequency increases. Thus the expected optimum, within the ranges that were tested, is at a pore size of 200 nm, a pressure of 4.5 bar and a frequency of 16 000 Hz.

Data from the sets of experiments, using tubular ceramic membranes, were combined, disregarding data obtained using the 100 nm membrane due to leakages affecting the data. It was determined that increasing the pressure, pore size and frequency lead to an increase in DO_2. It was determined, for this combined set of data, that the oxygen pressure and the frequency of the

sound wave vibrating the system has the most significant effect on the level of DO_2.

A difference in levels of DO_2 was observed when comparing the results of these experiments with the results obtained by Ahmed *et al.* (2018). It can be seen in Figure 2.13 that after about 10 *minutes* the dissolved oxygen level reaches a level of about 38 mg/L (28.6 mL/L). It is concluded that this higher level is due to the fact that in the experiments, done by Ahmed *et al.* (2018), a static container of water is used where the level of DO_2 can continue to rise as time passes. The setup is also open to atmosphere, therefore leaks would be more difficult to detect as large bubbles could escape the mixture. The possibility of leaks attributing to the relatively high levels of DO_2 is a possibility.

5.3 Conclusion: Results

The experimental setup end method, as described in Chapter 3 was used and a number of experimental sets were conducted. Experimental sets were designed using Box-Behnken and functions were fitted to the results. These functions were analysed using ANOVA to determine if they are reasonable representations of the data.

The functions were analysed te determine what the effect and how significant the effect of pore size, pressure and frequency are on the level of dissolved oxygen in water. A genetic algorithm was used to determine where the expected optimum of each function is.

Considering all the results as a whole, it can be concluded that pore size, pressure and frequency has an effect on the level of DO_2 in the water. When considering the literature, it is expected that the bubble size has a significant effect on the level of dissolved oxygen. Considering the results of these experiments it is suspected that the three variables used, all have an effect on the bubble size and this affects the level of DO_2 in the water. It is also suspected that the zeta potential has a effect on the dissolution of oxygen bubbles in water, as the zeta potential could serve as resistance to dissolution as it is a additional force keeping the oxygen intact.

Chapter 6

Conclusion

Being able to successfully oxygenate a human intravenously by means of oxygenation catheter could lead to countless lives being saved, as this could be a accessible and cost efficient means of blood oxygenation. The main challenges regarding intravenous oxygenation include the meeting the total amount of oxygen required by the human body and not forming large oxygen bubbles that could be fatal. The use of nano-bubbles were suggested and a set of experiments were designed to act as a baseline investigation to determine if this possibly could be a solution and if it needs to be investigated further.

The main objectives of the project was to *conduct a literature study*, *design an experiment* to investigate the oxygenation by means of membranes, to *design a inlet manifold* where oxygen is introduced into water through a membrane, to determine the effects of membrane nominal more size and oxygen inlet pressure on the oxygenation of water and to determine if sonic interference has an effect on the oxygenation of water. All these objectives were met.

Objective 1 was met in Chapter 2 where a literature study was conducted. The literature study investigates the pulmonary system including oxygen transport and the oxygen requirements of a human. Known blood oxygenation methods, namely extracorporeal membrane oxygenation (ECMO) and intravascular oxygenation (IVOX) are discussed to understand the advantages and disadvantages of these devices.

Mass transfer of gas into a bulk liquid is investigated to better understand the theory behind oxygen bubbles dissolving in water. The use of flat sheet membranes to oxygenate water is investigated as well as the methods used to conduct these experiments. The unique properties of nano-bubbles were investigated and it was determined, from literature, that nano-bubbles are neutrally buoyant, have increased gas dissolution rate, have a negative surface charge called zeta-potential and have a larger surface contact area compared to larger

bubbles when the same total volume of oxygen is used. The use of tubular ceramic membranes to generate nano-bubbles in water was investigated and according to Ahmed *et al.* (2018) this is possible.

Objective 2 was met in Section 3.2, where an experimental setup was designed that mimics the critical properties such as the volume flow rate and blood pressure. The system was designed to use water as a working fluid.

Objective 3 was met in Sections 3.3 and 3.4 where two different inlet manifolds were designed. The inlet manifold in Section 3.3 was designed to mount flat sheet membranes and the manifold in Section 3.4 was designed to mount the tubular ceramic membranes.

Objective 4 was met in Chapter 5, where the data obtained during experimentation was analysed and it was determined that both the nominal pore size of the membrane and the oxygen inlet pressure affect the oxygenation of the water.

Objective 5 was met in Chapter 5, where it was determined that the frequency, that is generated by the speaker to vibrate the system, has a significant effect on the dissolved oxygen levels of the water.

During experimentation relatively low levels of DO_2 were obtained. This could be due to the stability of nano-bubbles, as observed in experiments done by Meegoda *et al.* (2018). A reason for the low levels of DO_2 could be that a number of nano-bubble exist in the mixture, but are stable and neutrally buoyant (NanoMAX, 2019) in the water.

As the overarching aim of the project is to be able to sufficiently oxygenate a human intravenously. Considering the evidence obtained, it cannot be concluded that using membranes with nano-scale pores are a viable method for blood oxygenation, as the measured DO_2 obtained in water is relatively low. The main concern however is the formation of large oxygen bubbles.

Chapter 7

Recommendations

The work covered in this project gives valuable baseline research that could serve as a building block for future work towards the overarching aim of sufficiently oxygenating a human intravenously. Further research into the behaviour of nano-bubbles could be of great advantage, not only to the medical field, but also in water purification, agriculture, health and fitness and numerous other applications.

One of the properties of nano-bubbles are that they are neutrally buoyant and that due to their negative surface charge they can stay in a mixture for long periods of time, as illustrated by the experiment done by Meegoda *et al.* (2018). It is hypothesised that during experimentation, nano-bubbles were generated, but remain stable in the water. As these bubbles did not dissolve the dissolved oxygen levels does not reflect the available oxygen.

Another important consideration is the difference in the oxygen carrying capacity of blood and of water. As discussed in Section 2.1 and seen in Equation 2.3, the main component, attributing to the total dissolved oxygen in blood is haemoglobin. It is hypothesised that should nano-bubbles be generated in a fluid with a similar oxygen carrying capacity as blood, the suspended oxygen nano-bubbles will dissolve and the total dissolved oxygen level wil increase significantly.

7.1 PhD proposal

It is proposed that the research continues and the experimental setup be adjusted to work with fluid that has a similar oxygen carrying capacity as blood. It is suggested that a fluid of the perfluorocarbons group be used. In Figure 7.1, the proposed experimental setup is given. The setup is modified to be

closed loop, including a pump. The pump (C) and the ball valve next to it will be used to control the flow rate and pressure and mimic the conditions in a human body. A heat exchanger (B) is added to increase and keep the system temperature at $36°C$, which is the same as body temperature. This would be a significant addition to the research as temperature is expected to have a significant effect on oxygen dissolution. To remove the oxygen that is inserted into the system a nitrogen sparger is inserted into the buffer tank.

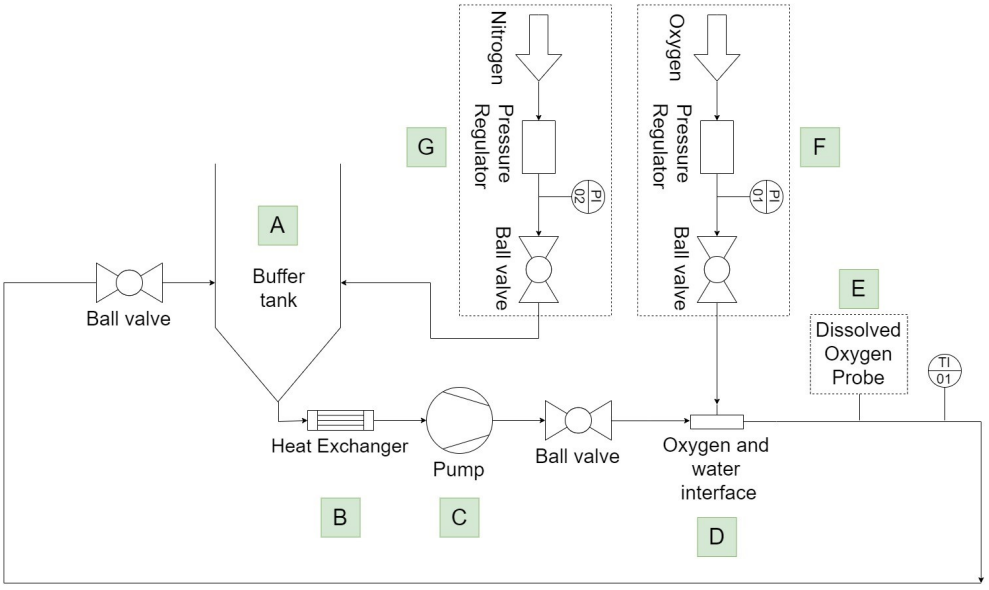

Figure 7.1: Schematic diagram of the proposed experimental setup including buffer tank (A), heat exchanger (B), positive displacement pump (C), oxygen inlet manifold (D), dissolved oxygen probe (E), oxygen tank with regulator (F) and nitrogen sparger setup (G)

It is proposed that samples be taken and the zeta potential and bubble size be determined and analysed. The same three independent variables are suggested, namely membrane pore size, oxygen inlet pressure and vibration frequency.

The proposed objectives of further research are:

1. To expand on the current *literature study* including research on perfluorocarbons, temperature dependence of oxygen mass transfer and other membrane alternatives as well as methods of validating nominal pore size and determining and observing bubble size (nano-scale).

2. To design an *experimental setup*, mimicking the pulmonary system with a working fluid that has a similar oxygen carrying capacity as blood.

3. To determine the effect of the nominal pore size of the membrane and the oxygen inlet pressure on the dissolved oxygen levels of a fluid with the same oxygen carrying capacity as blood.

4. To determine the effect of the nominal pore size of the membrane and the oxygen inlet pressure on the bubble size and zeta potential.

5. To determine the effect of sonic interference or alternative vibration technique on the dissolved oxygen levels of a fluid with the same oxygen carrying capacity as blood.

6. To determine the effect of sonic interference or alternative vibration technique on bubble size and zeta potential.

The research proposed will give valuable insight into the behaviour of nan-bubbles and would contribute to academia, as nano-bubbles have numerous applications.

Bibliography

Ahmed, A.K.A., Sun, C., Hua, L., Zhang, Z., Zhang, Y., Zhang, W. *&* Marhaba, T. 2018. Generation of nanobubbles by ceramic membrane filters: The dependence of bubble size and zeta potential on surface coating, pore size and injected gas pressure. *Chemosphere*, 203:327–335.

Anton-Paar. 2019. Litesizer 500 anton-paar 2019. `https://www.anton-paar.com/za-en/products/details/litesizertm-500/`, Online, accessed on 4 November 2019.

Carlsson, M., Andersson, R., Bloch, K.M., Steding-Ehrenborg, K., Mosan, H., Stahlberg, F., Ekmehag, B. *&* Arheden, H. 2012. Cardiac output and cardiac index measured with cardiovascular magnetic resonance in healthy subjects, elite athletes and patients with congestive heart failure. *Journal of Cardiovascular Magnetic Resonance*, 14(1).

Chaplin, M. 2019. Nanobubbles (ultrafine bubbles). `http://www1.lsbu.ac.uk/water/nanobubble.html`, Online, accessed on 12 November 2019.

Fourie, P. 2017. Oxygen delivery to the tissue and respiratory distress syndrome - intensive care continuous training.

Henley, E.J., Seader, J. *&* Roper, D.K. 2011. *Separation process principles*. 3rd edition. Wiley.

Leach, R.M. 2002. The pulmonary physician in critical care 2: Oxygen delivery and consumption in the critically ill. *Thorax*, 57(2):170–177.

Mallawaarachchi, V. 2020. Introduction to genetic algorithms - including example code.
Available at: `https://towardsdatascience.com/introduction-to-genetic-algorithms-in`

Mathworks.com, M. 2020.
Available at: `https://www.mathworks.com/help/gads/how-the-genetic-algorithm-works.`

MATLAB. 2019. Matlab.

Maynard, L.N. 2017. Development of an intravenous oxygenation membrane. Ph.D. thesis, Stellenbosch University.

Meegoda, J.N., Aluthgun Hewage, S. *&* Batagoda, J.H. 2018. Stability of nanobubbles. *Environmental Engineering Science*, 35(11):1216–1227.

Moleaer. 2019. Nanobubbles. `https://www.moleaer.com/nanobubbles`, Online, accessed on 12 November 2019.

NanoMAX. 2019. Nanobubbles explained - nanomax - advanced nanobubble generators. `https://www.nanomax.com.au/nanobubbles-explained/`, Online, accessed on 12 November 2019.
Available at: `https://www.nanomax.com.au/nanobubbles-explained/`

RStudio. 2019. Rstudio.

SANS. 2012. *South African National Standards. categorization and conformity assessment criteria for all pressure equipment (SANS 347-2012).* 2nd edition. SANS.

Scott, K. 2006. *Handbook of industrial membranes.* Elsevier Advanced Technology.

Stoecklein, H., Slack, S., Tonna, J.E. *&* Youngquist, S.T. 2019. Ecmo and ecpr - jems. `https://www.jems.com/2017/12/01/ecmo-ecpr/`, Online, accessed on 9 November 2019.

Sweeney, B. 2019. Extracorporeal membrane oxygenation (ecmo) in the ed. `http://www.emdocs.net/extracorporeal-membrane-oxygenation-ecmo-in-the-ed/`, Online, accessed on 9 November 2019.

Synderfiltration. 2019. Definition of molecular weight cut off. `https://synderfiltration.com/learning-center/articles/membranes/molecular-weight-cut-off`, Online, accessed on 1 November 2019.

TIBC. Statistica.

Treacher, D.F. *&* Leach, R.M. 1998. Abc of oxygen: Oxygen transport—1. basic principles. *BMJ*, 317(7168):1302–1306.

Yuan, S.-M. 2016. Lung replacement therapies for acute respiratory failure. *Signa Vitae - A Journal In Intensive Care And Emergency Medicine*, 12(1):19–22.

Appendix A

Statistical analysis results tables

A.1 Summary and ANOVA results for experimental setup using flat sheet membranes

Table A.1: Results table of the function fit to the data obtained using a flat sheet membrane

	Estimate	**Std. Error**	**t value**	**Pr(>|t|)**
Intercept	$1.272e^{-02}$	$1.316e^{+01}$	0.001	0.999
I(x_1^2)	$-1.200e^{-02}$	$8.086e^{-02}$	-0.148	0.887
$x1$	$1.050e^{-01}$	$2.024e^{+00}$	0.052	0.960
I(x_2^2)	$-2.560e^{-01}$	$3.234e^{-01}$	-0.792	0.459
$x2$	$1.432e^{+00}$	$1.471e^{+00}$	0.973	0.368
I(x_3^2)	$5.642e^{-08}$	$8.774e^{-08}$	0.643	0.544
$x3$	$-3.299e^{-04}$	$4.699e^{-04}$	-0.702	0.509

Table A.2: ANOVA table of the function fit to the data obtained using a flat sheet membrane

	Df	**Sum Sq**	**Mean Sq**	**F value**	**Pr(>F)**
$I(x_1^2)$	1	1.9097	1.90969	3.2714	0.1205
x_1	1	0.0000	0.00004	0.0001	0.9934
$I(x_2^2)$	1	0.6898	0.68975	1.1816	0.3188
x_2	1	1.1046	1.10457	1.8922	0.2181
$I(x_3^2)$	1	0.0150	0.01503	0.0257	0.8778
x_3	1	0.2876	0.28765	0.4928	0.5090
Residuals	6	3.5025	0.58375		

Table A.3: ANOVA of the function as described by Equation 5.3

	Df	**Sum Sq**	**Mean Sq**	**F value**	**Pr(>F)**
$I(x_1^2)$	1	1.90969	1.90969	2.5463	0.3564
x_1	1	0.00004	0.00004	0.0001	0.9952
$I(x_2^2)$	1	0.68975	0.68975	0.9197	0.5133
x_2	1	1.10457	1.10457	1.4728	0.4388
$I(x_3^2)$	1	0.01503	0.01503	0.0200	0.9105
x_3	1	0.28765	0.28765	0.3835	0.6470
$I(x_4^2)$	1	0.23390	0.23390	0.3119	0.6758
x_4	1	0.55990	0.55990	0.7465	0.5464
$I(x_5^2)$	1	0.46840	0.46840	0.6245	0.5742
x_5	1	1.48656	1.48656	1.9821	0.3932
$x4x5$	1	0.00373	0.00373	0.0050	0.9552
Residuals	1	0.74999	0.74999		

A.2 Summary and ANOVA results for experimental setup using tubular ceramic membranes

Table A.4: Results table of the function as described by Equation 5.7

	Estimate	**Std. Error**	**t value**	**Pr(> | t |)**
Intercept	$-5.656e^{-01}$	$8.267e^{-01}$	-0.684	0.5194
I(x_1^2)	$-7.863e^{-05}$	$3.743e^{-05}$	-2.100	0.0804
x_1	$1.948e^{-02}$	$9.676e^{-03}$	2.013	0.0907
I(x_2^2)	$4.611e^{-02}$	$8.190e^{-02}$	0.563	0.5938
x_2	$-2.472e^{-01}$	$4.147e^{-01}$	-0.596	0.5729
I(x_3^2)	$-2.170e^{-09}$	$3.199e^{-08}$	-0.068	0.9481
x_3	$8.394e^{-05}$	$1.713e^{-04}$	0.490	0.6416

Table A.5: ANOVA of the function as described by Equation 5.7

	Df	**Sum Sq**	**Mean Sq**	**F value**	**Pr(>F)**
I(x_1^2)	1	0.08685	0.08685	1.1191	0.33084
x_1	1	0.46997	0.46997	6.0556	0.04907
I(x_2^2)	1	0.00142	0.00142	0.0183	0.89673
x_2	1	0.03691	0.03691	0.4756	0.51620
I(x_3^2)	1	0.22498	0.22498	2.8989	0.13953
x_3	1	0.01863	0.01863	0.2400	0.64159
Residuals	6	0.46566	0.07761		

Appendix B

Pressure vessel design

In Figure B.1 the SANS 347-2012 Graph for vessels, containing non-dangerous gas, is given. The graph is an indication of the level of design and approval required for the design of a pressure vessel. The pressure vessel used in the experiments falls within the sound engineering practice (SEP) region, therefore it does not have to be designed or approved by a professional engineer.

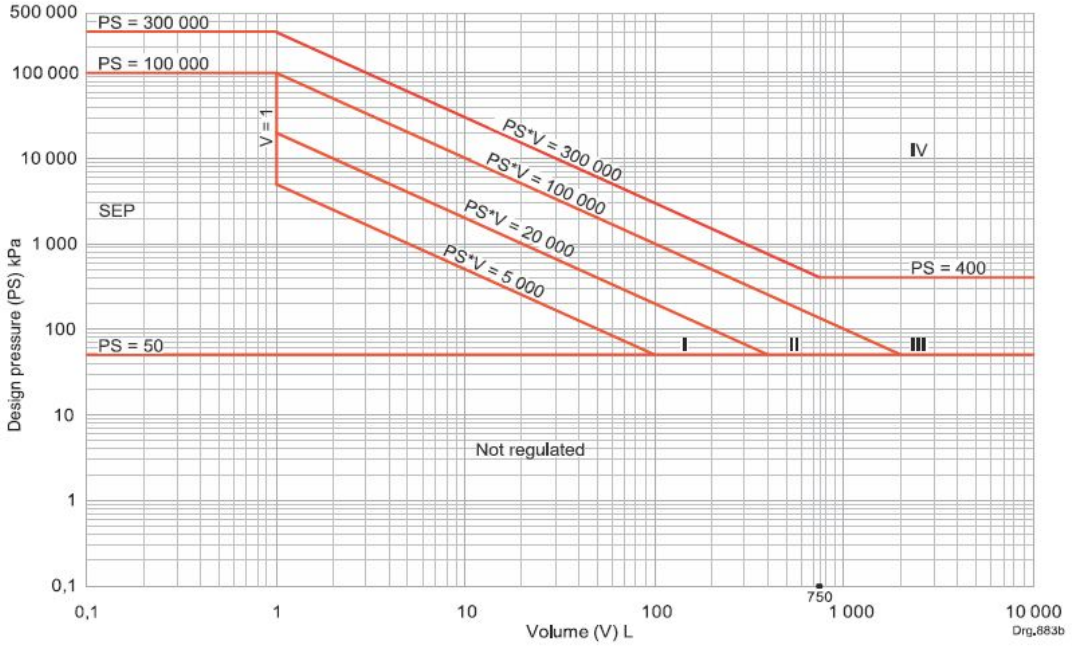

Figure B.1: SANS 347-2012 Graph for vessels, Non-dangerous gas (SANS, 2012)

To ensure the pressure vessel will withstand the pressures it will be subject to, a finite element analysis (FEA) of the vessel was done. The results of the FEA

can be seen in Figure B.2. It was determined that the minimum safety factor is 3.47. This means that the pressure vessel is 3.47 stronger that it needs to be to resist failure.

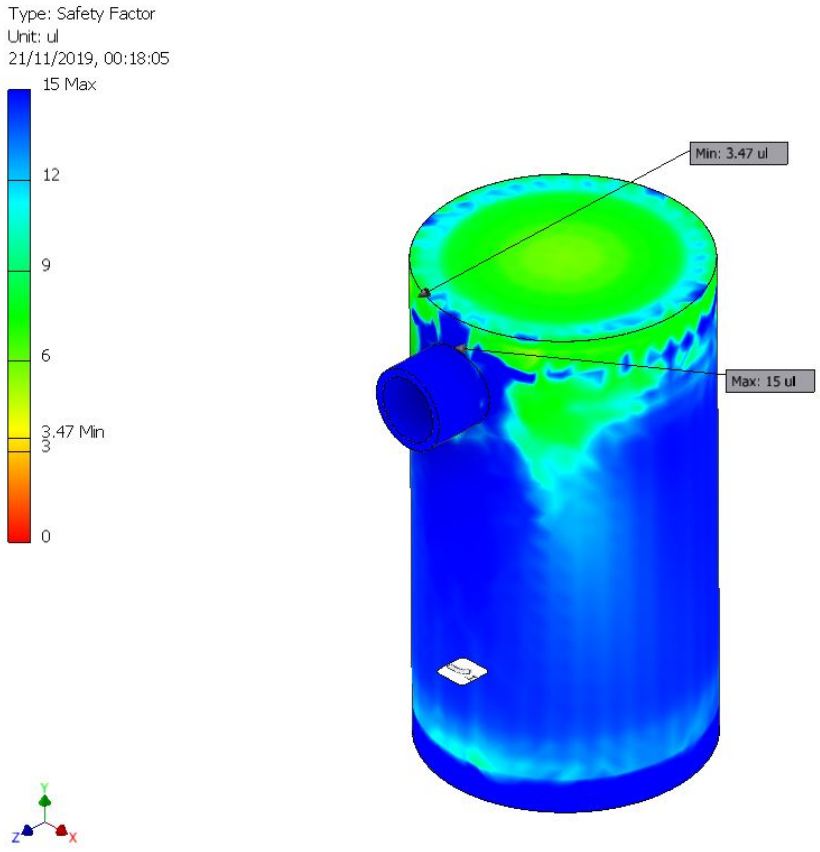

Figure B.2: Finite element analysis of the pressure vessel indicating the maximum and minimum safety factor at a pressure of 10 *bar*

Appendix C

Scanning electron microscope results

This Appendix includes larger images of the results obtained during the scanning electron microscope analysis of the flat sheet membranes.

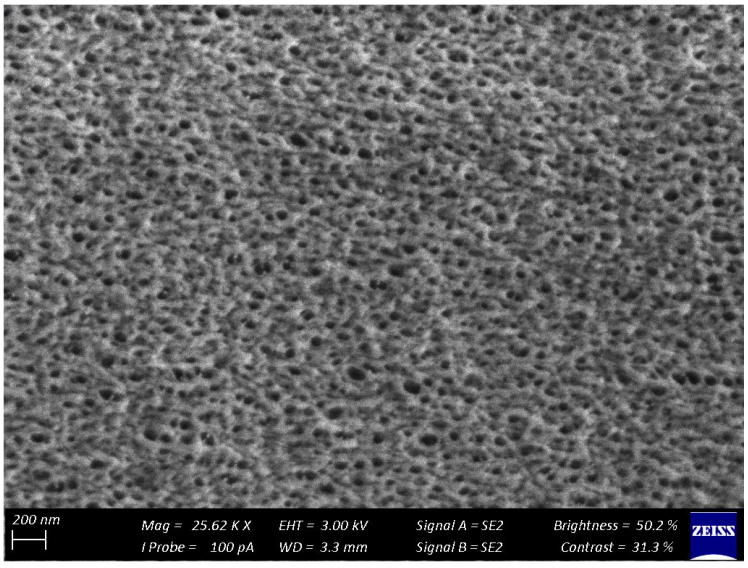

Figure C.1: Scanning electron microscope image of TRISEP® UB70

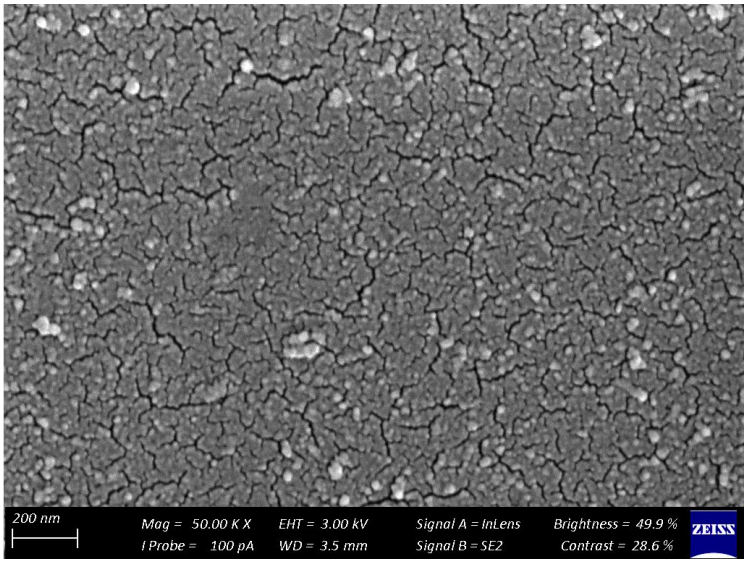

Figure C.2: Scanning electron microscope image of SelRO® MPS-34

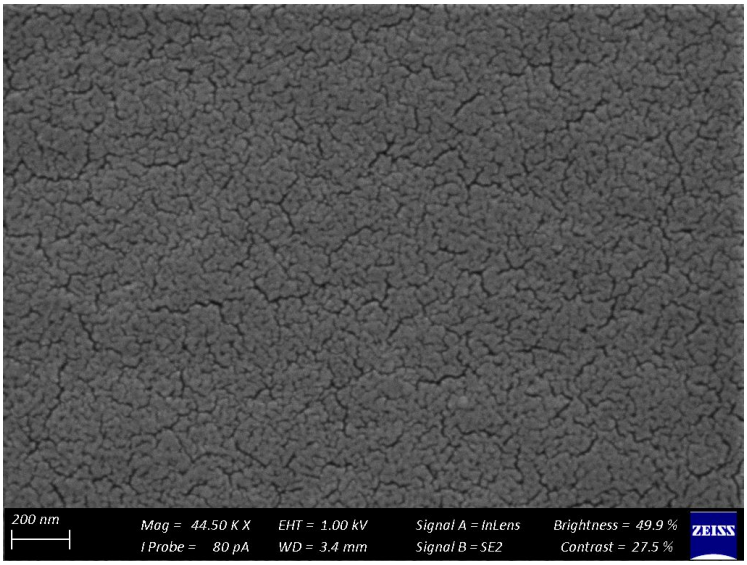

Figure C.3: Scanning electron microscope image of NADIR® UH050 P

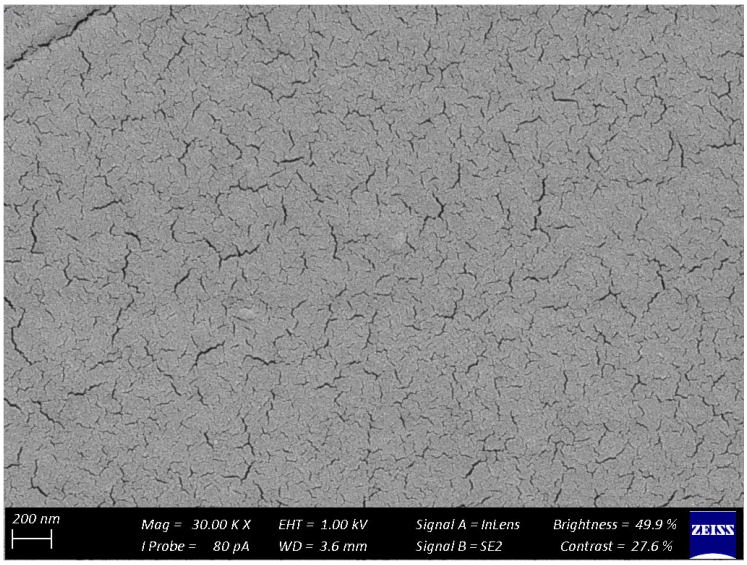

Figure C.4: Scanning electron microscope image of NADIR® UH010 P